JNeurosci
THE JOURNAL OF NEUROSCIENCE

Research Articles | Behavioral/Cognitive

Saccade direction and distractor location jointly drive spatial asymmetries in saccadic inhibition

https://doi.org/10.1523/JNEUROSCI.1289-26.2026

Received: 27 July 2026
Revised: 11 November 2026
Accepted: 15 November 2026

Copyright © 2026 the authors

This Early Release article has been peer reviewed and accepted, but has not been through the composition and copyediting processes.The final version may differ slightly in style or formatting and will contain links to any extended data.

Alerts: Sign up at www.jneurosci.org/alerts to receive customized email alerts when the fully formatted version of this article is published.

Saccade direction and distractor location jointly drive spatial asymmetries in saccadic inhibition

Abbreviated title: **Spatial asymmetries in saccadic inhibition**

Jiacheng Hao[1,2], David Melcher[2,4] & Marisa Carrasco[1,3]

[1]Department of Psychology, New York University, New York, NY, USA

[2]Department of Psychology, New York University Abu Dhabi, United Arab Emirates

[3]Center for Neural Sciences, New York University, New York, NY, USA

[4]Center for Brain & Health, New York University Abu Dhabi, United Arab Emirates

Correspondence should be addressed to Jiacheng Hao at jiacheng.hao@nyu.edu or Marisa Carrasco at marisa.carrasco@nyu.edu

Competing Interest Statement: The authors declare no competing interests.

JNeurosci Accepted Manuscript

Abstract

Saccadic inhibition (SI), the transient suppression of saccade generation following an abrupt visual transient (distractor), clearly demonstrates how sensory input interrupts ongoing oculomotor preparation. SI typically peaks 90–100 ms after transient onset, followed by a rebound in saccade probability. SI depends on distractor properties and its spatial relation to the planned saccade. However, it is unknown whether SI is spatially anisotropic across polar angles and whether such anisotropy is driven by the planned saccade endpoint, the distractor location, or their configuration. Sixteen human observers (8 female) completed two experiments, making speeded saccades to Gabor targets while a task-irrelevant Gabor distractor appeared shortly after target onset. In Experiment 1, saccade targets appeared at cardinal and distractors at intercardinal locations; Experiment 2 reversed this arrangement. Distractor-present trials were compared with target-location-matched no-distractor baselines to quantify SI strength and timing. Across experiments, distractors elicited a canonical SI profile. In Experiment 1, inhibition strength showed independent effects of both target and distractor locations: upward saccades were the most resistant to inhibition, while inhibition was stronger, earlier, and broader by upper-field than lower-field distractors. In Experiment 2, inhibition strength showed a reliable target-by-distractor interaction, with the strongest upper-distractor effect emerging for upper-field saccade targets. Across experiments, the timing of maximal inhibition was driven primarily by distractor location, while rebound dynamics

Neurosci Accepted Manuscript

mirrored inhibition strength. These findings reveal that SI is shaped by target–distractor configuration and exhibits an upper-field distractor advantage.

Significance

Sudden visual events interrupt our planned eye movements. This interruption is often considered a global, uniform pause in the brain's oculomotor program. This study challenges that assumption by demonstrating that saccadic inhibition is highly sensitive to the exact spatial layout of both the intended eye movement and the distracting visual stimulus. Specifically, we show that upward eye movements are highly resistant to disruption, whereas distractors in the upper visual field exert the strongest inhibition, particularly when paired with upper-field targets. These findings reveal that sensorimotor gating in the brain is not a blanket suppression mechanism, but rather a tuned, asymmetric process. These findings provide critical insights into how the brain dynamically prioritizes competing visual inputs during active vision.

JNeurosci Accepted Manuscript

Keywords: eye movements, saccadic inhibition, polar-angle asymmetries, visual field

Introduction

Humans sample visual information by alternating eye fixations and rapid saccades toward relevant locations. In dynamic environments, new sensory input often occurs during saccade preparation, interrupting ongoing oculomotor programming to delay or suppress impending eye movements. This interruption causes saccadic inhibition (SI): a time-locked reduction in saccade frequency following a transient onset, peaking at ~90–110 ms before rebounding to baseline (**Fig.1**). Because SI is reliable and involuntary across oculomotor contexts, it provides a robust behavioral assay of how visual input interacts with saccade preparation (Reingold & Stampe, 1999, 2002, 2004; Buonocore & McIntosh, 2008; Edelman & Xu, 2009; Bompas et al., 2020).

SI strength and timing depend on interactions between transient sensory properties—size, location, contrast, spatial frequency, orientation, and motion (Stampe & Reingold, 2002; Buonocore & McIntosh, 2012; Khademi et al., 2023)—and oculomotor state, shaped by task context, behavioral relevance, and attentional allocation (Reingold & Stampe, 2004; Buonocore & McIntosh, 2013). Spatial factors also shape SI. In visually guided saccade protocols, inhibition profiles depend on target-relative positions such as ipsilateral versus contralateral or near versus remote distractors (Buonocore & McIntosh, 2008, 2012; Edelman & Xu, 2009; Walker & Benson, 2013, 2015). However, most protocols use restricted geometries, typically testing stimuli along the horizontal axis. Consequently, whether SI spatial modulation reflects only target–distractor geometry or varies systematically with polar angle remains unknown.

This gap is critical because visual processing is strongly anisotropic across the visual field. Sensitivity declines with eccentricity and varies with polar angle. Observers typically perform better along the horizontal than the vertical meridian—the horizontal–vertical anisotropy—and

JNeurosci Accepted Manuscript

better along the lower than the upper vertical meridian—the vertical meridian asymmetry. These polar-angle asymmetries occur at threshold and suprathreshold levels across many dimensions, including contrast sensitivity, spatial resolution, acuity, and motion (review, Himmelberg et al., 2023b). Temporal dynamics mirror these spatial asymmetries; information accrues faster along the horizontal than vertical meridian and along the lower than upper vertical meridian (Carrasco et al., 2004). They are also reflected in non-uniform retinal sampling (Curcio et al., 1990; Curcio & Allen, 1990; Kupers et al., 2019, 2022) and V1 cortical surface area (Silva et al., 2018; Benson et al., 2021; Himmelberg et al., 2021, 2022, 2023a, 2025).

However, the neural information underlying these perceptual measures may differ from the rapid visual signals that interrupt saccade preparation. Whereas perceptual tasks typically involve accumulating and integrating visual information for discrimination, SI may be particularly sensitive to early visual transients reaching oculomotor circuits (Bompas & Sumner, 2011; Bompas et al., 2020). Indeed, visual-field asymmetries extend into the perisaccadic interval but depend on the computations probed. Presaccadic attention exacerbates asymmetries in contrast sensitivity (Hanning et al., 2022, 2024) and the contrast sensitivity function (Kwak et al., 2024), whereas peripheral preview reduces them (Liu et al., 2024). Several factors could drive spatial anisotropies in SI. In the superior colliculus (SC) and brainstem, visual transients and preparatory motor signals converge, perturbing oculomotor programming and rise-to-threshold dynamics (Bompas & Sumner, 2011; Jantz et al., 2013; Salinas & Stanford, 2018; Bompas et al., 2020; Buonocore et al., 2021). The SC receives direct retinal and cortical input and projects to premotor brainstem circuits controlling saccades (Isa & Hall, 2009; Basso & May, 2017). Vertical asymmetries in SC receptive-field tuning vary across species (Hoy & Farrow, 2025), with smaller receptive fields and faster responses reported in the upper visual field of non-human primates (Hafed & Chen, 2016). However, human SC asymmetries remain unexplored. Because human and monkey perceptual

JNeurosci Accepted Manuscript

asymmetries can differ, likely reflecting distinct ecological niches (Tünçok et al., 2025), the neural basis of human SI remains open. Consequently, human SI could reflect polar-angle biases inherited from retinal or cortical representations, intrinsic oculomotor anisotropies, or their interactions.

If SI spatial variation is influenced primarily by asymmetries in distractor sensory processing, then distractor-evoked latency or strength differences should alter SI timing or magnitude (Bompas & Sumner, 2008; Buonocore & McIntosh, 2012). Conversely, if SI magnitude is shaped mainly by the oculomotor plan, it should vary with saccade direction or target–distractor geometry. Distinguishing these contributions requires independently manipulating target and distractor locations.

Here, we tested whether SI varies with polar angle across two complementary experiments. Experiment 1 placed targets on the cardinal axes and distractors at intercardinal locations to test whether SI depends on planned saccade direction at matched distractor eccentricities. Experiment 2 reversed this geometry—placing targets at intercardinal locations and distractors on the cardinal axes—to evaluate whether SI depends on distractor polar angle and whether this dependence changes with saccade endpoint. Together, these experiments map how target and distractor locations shape the SI profile.

JNeurosci Accepted Manuscript

Materials and Methods

Experiment 1: Cardinal targets and intercardinal distractors

Observers

Sixteen human observers (8 male; age range, 22–36 years) with normal or corrected-to-normal vision participated in Experiment 1. All observers reported no history of neurological or psychiatric disorders and provided written informed consent before participation. One observer was an author (J.H.). The protocol was approved by the New York University Institutional Review Board and was conducted in accordance with the Declaration of Helsinki.

Apparatus

Testing was conducted in a dimly lit room. Observers viewed the display with head position stabilized by a combined chin and forehead rest. Stimuli were presented on a gamma-corrected 20-inch CRT monitor (ViewSonic G220fb; 1,280 × 960 pixels; 100 Hz) at a viewing distance of 79 cm. The background was uniform mid-gray, with a mean luminance of approximately 26 cd/m². Eye position was recorded monocularly from the right eye using an EyeLink 1000 Desktop Mount system (SR Research, Ottawa, Canada), sampling at 1000 Hz and controlled through the EyeLink Toolbox for MATLAB and Psychtoolbox (Cornelissen et al., 2002). Each session began with a standard 9-point calibration and validation procedure; drift correction or recalibration was performed whenever necessary.

Stimuli and Design

Stimuli were generated in MATLAB (MathWorks, Natick, MA) using Psychtoolbox-3 (Brainard, 1997; Pelli, 1997) and were presented on the mid-gray background. Saccade targets and distractors were black-and-white Gabor patches with the same carrier phase of 0 cycles, windowed by circular Gaussian envelopes. Targets were 2.8° in diameter, had a Gaussian-envelope standard deviation of 0.33° and a spatial frequency of 5.5 cycles/deg, and were

JNeurosci Accepted Manuscript

presented at 64% Michelson contrast. These target parameters were chosen to provide clearly localizable peripheral Gabor targets at 8.5° eccentricity, within the range typically used in previous presaccadic-attention and visual-field-asymmetry studies (Hanning et al., 2022, 2024; Kwak et al., 2024, 2025). Distractors were larger Gabor patches, 6° in diameter, had a Gaussian-envelope standard deviation of 0.71° and a spatial frequency of 2 cycles/deg and 80% Michelson contrast presented at 8.5° eccentricity. Because SI is sensitive to the physical strength and feature content of the eliciting transient, distractor parameters were selected from pilot testing to elicit a robust SI profile while avoiding floor or ceiling effects in SI strength.

We used a within-observer design in which saccade target location and distractor location were varied factorially on distractor-present trials. Saccade targets appeared at 8.5° eccentricity at one of four cardinal locations: upper (UVM), lower (LVM), left (LHM), or right (RHM). Distractors appeared at the same eccentricity at one of four intercardinal locations: upper right, upper left, lower left, or lower right. No-distractor trials were interleaved with distractor-present trials and served as target-location-matched baselines for SI computation.

This cardinal-target/intercardinal-distractor geometry separated the two spatial factors of interest. Placing saccade targets along the cardinal axes allowed us to test whether the direction of the planned eye movement modulated SI, whereas placing distractors at intercardinal locations allowed us to estimate how the location of an abrupt visual transient shaped the SI response.

Each observer completed 200 trials for each of the 20 pairings of target location and distractor condition: four target locations crossed with four distractor locations and the no-distractor baseline. This yielded 4,000 experimental trials per observer in total.

JNeurosci Accepted Manuscript

198

199 **Procedure**

200

201 Figure 2 shows the shared trial procedure and the spatial configurations used in Experiments
202 1 and 2. To estimate baseline saccadic reaction times separately for each observer and target
203 location, before the main experiment, observers completed two no-distractor calibration blocks
204 of 100 trials each, one with targets restricted to the vertical axis and one with targets restricted
205 to the horizontal axis (50 per location). Calibration trials were used only to determine the
206 observer and target location specific target–distractor stimulus onset asynchrony (SOA) for
207 the main experiment and were not included in the 4,000-trial experimental dataset.

208

209 For each observer and target location, we computed the median calibration saccadic reaction
210 time (SRT). For Experiment 1, the group-average median baseline SRTs were 196.0 ms for
211 upward targets, 212.3 ms for downward targets, 184.5 ms for leftward targets, and 188.0 ms
212 for rightward targets (Fig. 3A, solid line). For comparison, we plot the group-average
213 medianSRTs of the calibration condition (Fig. 3A, dotted line). The values are positively and
214 significantly correlated (Pearson $r(62) = .95$, $p = 6.49 \times 10^{-33}$; Supplemental Fig. S1). To assess
215 the stability of location-dependent SRT differences, calibration and main-session no-distractor
216 SRTs were separately z-scored across the four target locations within each observer. The
217 correlations remained strong in both experiments (Experiment 1: $r(62) = .888$, $p < .0001$;
218 Experiment 2: $r(62) = .881$, $p < .0001$; within-observer permutation tests, both $p < .001$;
219 Supplemental Fig. S2).

220

221 On distractor-present trials in the main experiment, the distractor appeared after target onset
222 at an SOA equal to the observer's median calibration SRT for that target location minus 90
223 ms. This timing was chosen so that the expected SI minimum, which typically occurs

JNeurosci Accepted Manuscript

approximately 90 ms after an abrupt visual transient, would fall near the peak of the observer's baseline saccade-latency distribution for that target location.

Each trial began with a central fixation dot (0.15° radius) presented on the gray background. Gaze position was monitored online, and the trial sequence proceeded only after fixation was maintained within a 1.75° radius around fixation for a jittered interval of 0.9–1.5 s. A peripheral Gabor target then appeared for 400 ms at one of the four cardinal locations. Observers were instructed to make a saccade to the target as quickly and accurately as possible.

On distractor-present trials, a Gabor distractor appeared after target onset according to the observer- and target-location-specific SOA determined from the calibration blocks. The distractor remained onscreen for 250 ms and overlapped temporally with the target. On no-distractor trials, no visual transient was presented after target onset. After the saccade response, observers returned gaze to fixation and initiated the next trial with a self-paced keypress, followed by a 0.7-s inter-trial interval.

The main experiment was completed across four sessions. Each session consisted of 10 blocks of 100 trials, for a total of 40 blocks and 4,000 experimental trials. Within each block, targets were restricted to one cardinal axis: either the vertical axis, containing upward and downward saccade targets, or the horizontal axis, containing leftward and rightward saccade targets. The four distractor locations and the no-distractor baseline condition were randomly interleaved within each block. Vertical- and horizontal-axis blocks were interleaved across the experiment, and trial counts were balanced across target locations and distractor conditions.

JNeurosci Accepted Manuscript

If gaze deviated from the fixation window, the trial was aborted and appended to the end of the block. Repeated fixation failures prompted drift correction or recalibration.

Eye-movement preprocessing

Saccade events were detected using the EyeLink event parser with the default thresholds used during recording: velocity threshold, 30°/s; acceleration threshold, 8000°/s². EDF files were read offline in MATLAB using SR Research EDFMEX, and trial selection and analyses were performed within MATLAB. For each trial, we identified the first saccade initiated after target onset and defined its onset latency relative to target onset as the saccadic reaction time. Trials were excluded if no saccade was detected after target onset (0.25%), if the saccadic reaction time was shorter than 70 ms (to exclude anticipatory responses unlikely to be visually guided) or longer than 500 ms (2.89%), if the first saccade had an amplitude smaller than 1° of visual angle (1.80%), or if the first saccade was not directed toward the instructed target location (0.38%). Thus, 94.69% of the trials were analyzed, with comparable numbers between distractor-present (94.59%) and distractor-absent conditions (95.07%).

To assess whether directional errors were more common on distractor-present trials, we fitted a binomial logistic mixed-effects model to trials reaching the direction criterion, with directional error as the binary outcome, distractor presence as a fixed effect, and participant as a random intercept. For distractor-present directional errors, we tested whether saccades were preferentially directed toward the distractor using a participant- and target-location stratified permutation test. The primary SI analysis focused on target-directed saccades to characterize the interruption of the instructed saccade plan. To assess the influence of this exclusion criterion, we repeated the analysis after restoring otherwise eligible trials excluded solely because of saccade direction.

JNeurosci Accepted Manuscript

To verify that the retained saccades were target-directed, endpoint error vectors were computed relative to the target center. Endpoint distributions were visualized as normalized frequency maps averaged across observers for each target configuration (**Fig. 3B,** left).

SI profiles were constructed in MATLAB separately for each observer and spatial condition. For distractor-present trials, saccade onset times were re-expressed relative to distractor onset. For no-distractor trials from the main experiment, a pseudo-distractor onset was assigned using the same observer- and target-location-specific SOA used for distractor-present trials. This procedure aligned no-distractor baseline trials to the same temporal reference as distractor-present trials.

For each observer, saccade target location, and distractor location, we constructed a distractor-aligned saccadic frequency distribution using 1-ms bins. Bin counts were divided by the number of valid trials in that condition and expressed as a percentage of trials. The corresponding no-distractor baseline distribution was constructed from no-distractor trials from the same observer and saccade target location, aligned to the pseudo-distractor onset. The SI profile was then computed as the difference between the distractor-present distribution and the matched no-distractor baseline distribution:

$$SI(t) = \text{distractor-present saccade frequency}(t) - \text{no-distractor baseline saccade frequency}(t).$$

Negative values of SI(t) indicate a reduction in saccade frequency following distractor onset, whereas positive values indicate a rebound above baseline. Difference profiles were smoothed with a 31-ms moving-average window before parameter extraction. This window

JNeurosci Accepted Manuscript

299 approximated the temporal smoothing scale used in previous SI studies while adapting the
300 procedure to the 1-ms binning resolution of the present data (Buonocore & McIntosh, 2008,
301 2012, 2013; Bompas & Sumner, 2011). This target-location-matched baseline procedure
302 ensured that distractor-location effects were estimated relative to the appropriate baseline
303 saccade-latency distribution for each planned saccade direction.

304

305 For each observer, saccade target location, and distractor location condition, we extracted
306 nonparametric measures describing the strength, timing, and temporal extent of SI. Inhibition
307 strength was defined as the minimum value of the SI profile, and dip latency as the time of
308 maximal inhibition relative to distractor onset. The temporal width of inhibition was measured
309 as the full width at half minimum, defined by the first post-distractor crossing of 50% dip depth
310 and the subsequent return to that criterion after the minimum (Buonocore & McIntosh, 2008,
311 2012, 2013; **Fig. 1**). Crossing times were estimated by linear interpolation between adjacent
312 time bins.

313

314 To characterize the earliest detectable inhibition alongside maximal inhibition, we estimated
315 dip onset for each observer, saccade target location, and distractor location, following Bompas
316 and Sumner (2011) and Bompas et al. (2020). Saccade-latency distributions were constructed
317 using 4-ms bins, interpolated to 1-ms resolution, and smoothed with a 7-ms Gaussian window
318 (*SD* = 3 ms). At each time point, the distraction ratio was calculated as the difference between
319 the matched no-distractor and distractor-present distributions, divided by the matched no-
320 distractor distribution. The peak of the inhibitory episode was defined as the first maximum of
321 this ratio within the 70–150 ms post-distractor window, provided that the ratio exceeded 20%
322 and the difference between the distributions exceeded the equivalent of two saccades. Dip
323 onset was then estimated by tracing backward from this peak to the point at which the
324 distraction ratio fell below 2%, with the crossing time determined by linear interpolation.

JNeurosci Accepted Manuscript

Recovery following the inhibitory dip was quantified from the subsequent positive deflection of the SI profile. Rebound peak amplitude was defined as the maximum positive value following the inhibitory minimum, and rebound peak latency was defined as the time of this maximum relative to distractor onset. Rebound recovery slope was defined as the change in SI from the inhibitory minimum to the rebound peak divided by the time interval between these two points. To interpret slope effects, rebound recovery was further decomposed into its vertical component, the inhibitory minimum to rebound peak recovery amplitude, and its temporal component, the corresponding recovery interval. Rebound duration was defined as the contiguous post-minimum interval during which the SI profile remained above baseline around the rebound peak and was treated as a secondary measure.

Statistical Analysis

Primary analyses were conducted on individual-level SI measures. For each measure, we fit a linear mixed-effects model with saccade target location, distractor location, and their interaction as fixed effects, and observer as a random intercept. Models were fitted in MATLAB R2024a Update 5 using the Statistics and Machine Learning Toolbox version 24.1. Parameters were estimated by maximum likelihood, and fixed effects were evaluated with *F* tests using Satterthwaite-approximated degrees of freedom. When interactions were reliable, simple-effects analyses characterized the effect of distractor location within each saccade target location and the reciprocal effect of saccade target location within each distractor location. Pairwise follow-up comparisons were corrected using the Holm procedure within each comparison family.

JNeurosci Accepted Manuscript

Bayesian model comparisons assessed whether spatial effects were better described by additive effects of saccade target location and distractor location, in which each factor contributed independently to SI, or by their interaction, in which the effect of one factor depended on the other. Analyses were performed in R 4.5.3 using the BayesFactor package version 0.9.12.4.8. For each SI measure, an additive model containing the two main effects was compared with an interaction model that also included the saccade target location × distractor location interaction. The two models used the same repeated-measures structure. Fixed effects used the medium prior scale ($r = 0.5$), and random effects used the nuisance prior ($r = 1$). Bayes factors are reported as BF_{01}, defined as the evidence for the additive model relative to the interaction model; values greater than 1 therefore favor the additive model (Wagenmakers et al., 2018).

Repeated-measures ANOVAs with saccade target location and distractor location as within-observer factors were conducted as robustness checks on the primary mixed-effects analyses. As a convergent check, SI profiles were also summarized with parametric fits containing a baseline term and a negative-going Gaussian component, yielding fit-derived estimates of dip amplitude, dip latency, and dip width. These fit-derived measures were used to assess whether effects observed in the nonparametric SI measures were preserved under a compact description of the SI profile.

For frequentist tests, statistical significance was evaluated at α = .05. For post hoc pairwise comparisons and simple-effects analyses, reported *p* values are Holm-adjusted. Effect magnitudes are reported as model-estimated condition means or pairwise differences.

Experiment 2: Intercardinal targets and cardinal distractors

JNeurosci Accepted Manuscript

To investigate whether the spatial organization of SI depended only on whether cardinal visual-field locations were occupied by the planned saccade target, as in Experiment 1, or also by the cardinal location of the abrupt visual distractor, we reversed the locations of targets and distractors in Experiment 2 (Fig. 2C).

Observers

The same sixteen observers who completed Experiment 1 participated in Experiment 2.

Apparatus

The testing equipment and setting were identical to that used in Experiment 1.

Stimuli and design

Experiment 2 used the same stimulus parameters, temporal structure, eccentricity, contrast settings, and procedure as Experiment 1, but reversed the spatial assignment of saccade targets and distractors. Saccade targets appeared at 8.5° eccentricity at one of four intercardinal locations: upper right, upper left, lower right, or lower left. Distractors appeared at the same eccentricity at one of four cardinal locations: upper, lower, left, or right. No-distractor trials were interleaved to provide target-location-matched baseline saccade-latency distributions.

Timing calibration and procedure

JNeurosci Accepted Manuscript

The timing-calibration procedure was identical to Experiment 1, except that calibration SRTs were estimated for intercardinal target locations. Before the main experiment, observers completed two no-distractor calibration blocks of 100 trials each. One block contained the two upper-field target locations, and the other contained the two lower-field target locations. These 200 calibration trials were used only to estimate observer- and target-location-specific median SRTs for setting the distractor SOA in the main experiment and were not included in the 4,000-trial experimental dataset.

The group-average median calibration SRTs were 178.25 ms for upper-right targets, 171.5 ms for upper-left targets, 186.5 ms for lower-left targets, and 199.5 ms for lower-right targets (**Fig. 3A**, right panel). On distractor-present trials, the SOA was set to the observer's median calibration SRT for that target location minus 90 ms, so that the expected SI minimum would fall near the peak of the baseline saccade-latency distribution for that target location.

The trial sequence was otherwise identical to Experiment 1 (**Fig. 2A**). The main experiment was completed across four sessions. Each session consisted of 10 blocks of 100 trials, for a total of 40 blocks and 4,000 experimental trials. Within each block, targets were restricted to either the two upper-field target locations or the two lower-field target locations. The four distractor locations and the no-distractor baseline condition were randomly interleaved within each block. Upper- and lower-field target blocks were interleaved across the experiment, and trial counts were balanced across target locations and distractor conditions.

Eye-movement preprocessing and SI analysis

JNeurosci Accepted Manuscript

Eye-movement preprocessing, SI profile construction, parameter extraction, and statistical analyses followed the same procedures as in Experiment 1. After preprocessing, 95.10% of trials were retained, including 95.83% of distractor-absent trials and 94.92% of distractor-present trials. The same analyses of directional errors and the same sensitivity analysis were conducted as in Experiment 1. Endpoint distributions were visualized as normalized frequency maps averaged across observers for each target configuration (**Fig. 3B**, right panel).

The SI profiles were constructed separately for each observer and spatial condition as in Experiment 1.

Statistical analysis

We used linear mixed-effects models with saccade target location, distractor location, and their interaction as fixed effects, and observer as a random intercept. Bayesian additive-versus-interaction model comparisons, repeated-measures ANOVAs, and Gaussian-fit analyses were conducted using the same framework as in Experiment 1.

Results

Experiment 1: Cardinal targets and intercardinal distractors

Inhibition Analysis

JNeurosci Accepted Manuscript

We first verified that the abrupt visual distractors elicited reliable SI. When saccade onset distributions were aligned to distractor onset and compared with matched no-distractor baselines, distractor-present trials showed the expected transient reduction in saccade frequency followed by a brief rebound (**Fig. 4A**). This profile was evident in the group-average time course and across saccade target and distractor locations (**Fig. 5**), confirming that the distractors reliably interrupted ongoing saccade preparation.

For each SI parameter, we used linear mixed-effects models with fixed effects of saccade target location, distractor location, and their interaction, and a random intercept for observer. Post hoc comparisons were Holm-adjusted for multiple comparisons. Inhibition strength, indexed by the minimum of the SI profile, was spatially anisotropic in Experiment 1 (**Fig. 6**, top row). It varied with saccade target location, $F(3, 240) = 21.45$, $p = 2.41 \times 10^{-12}$, and distractor location, $F(3, 240) = 15.56$, $p = 2.78 \times 10^{-9}$, and these factors did not interact, $F(9, 240) = 0.84$, $p = .582$; $BF_{01} = 1.34$.

Given the lack of interaction, we analyzed target- and distractor-location effects separately. Saccade target location (**Fig. 5A**) indicated that inhibition was weakest for upward saccades and strongest for rightward saccades: Holm-adjusted comparisons (**Fig. 6A, top row**) showed that rightward saccades (−0.573 ± 0.048 percentage points (pp)) reflected stronger inhibition than leftward saccades (−0.485 ± 0.042 pp, $p = .0014$), downward (−0.478 ± 0.024 pp, $p = 2.86 \times 10^{-6}$), and upward saccades (−0.391 ± 0.034 pp, $p = 4.48 \times 10^{-13}$). Leftward and downward saccades also reflected stronger inhibition than upward saccades ($p = 6.82 \times 10^{-5}$; $p = .0108$, respectively). Thus, the inhibitory interruption of saccade preparation was nonuniform across saccade directions.

JNeurosci Accepted Manuscript

Distractor location (**Fig. 5B**) also produced non-uniform effects (**Fig. 6B top row**). Upper-field distractors (−0.551 ± 0.035 pp upper-right, −0.540 ± 0.037 pp upper-left) elicited stronger inhibition than lower-field distractors (−0.421 ± 0.028 pp lower-left, and −0.432 ± 0.028 pp lower-right distractors). All upper-versus-lower comparisons survived Holm adjustment, whereas left and right comparisons within the same vertical field did not differ (both $p = 1.000$).

The distractor-location effect was organized primarily by vertical position, with upper-field distractors producing stronger inhibition than lower-field distractors.

The timing of maximal inhibition showed a more selective spatial pattern (**Fig. 6**, second row). Dip latency varied with distractor location, $F(3, 240) = 8.68$, $p = 1.72 \times 10^{-5}$, but not with saccade target location, $F(3, 240) = 1.47$, $p = .224$, and these factors did not interact, $F(9, 240) = 1.34$, $p = .215$. Bayesian model comparison weakly favored the additive model, $BF_{01} = 1.89$.

Maximal inhibition occurred earlier for upper-field distractors (upper-right, 94.67 ± 2.25 ms; upper-left, 93.19 ± 2.31 ms) than for lower-field distractors (lower-left, 98.06 ± 1.70 ms; lower-right, 101.78 ± 2.30 ms). Holm-adjusted comparisons showed earlier inhibitory minima for upper-left than lower-right and lower-left distractors, and for upper-right than lower-right distractors. These significant differences ranged from 4.88 to 8.59 ms, all adjusted $p \leq .0145$. Upper-field distractors therefore produced both stronger and earlier inhibition.

Dip onset showed a similar spatial pattern (**Fig. 6**, bottom row). Onset varied with distractor location, $F(3, 238.01) = 12.98$, $p = 6.99 \times 10^{-8}$, but not with saccade target location, $F(3, 238.01) = 1.67$, $p = .174$, and these factors did not interact, $F(9, 238.01) = 0.93$, $p = .497$.

JNeurosci Accepted Manuscript

Holm-adjusted comparisons showed earlier onset for upper-right than lower-left (7.93 ms, p = .00579) and lower-right distractors (12.40 ms, $p = 8.85 \times 10^{-6}$), and for upper-left than lower-left (8.96 ms, p = .00191) and lower-right distractors (13.42 ms, $p = 1.53 \times 10^{-6}$). Onset did not differ reliably between the two upper-field or the two lower-field distractor locations (both $p \geq .155$). Thus, consistent with dip latency, upper-field distractors produced earlier inhibition onset than lower-field distractors.

The temporal width of inhibition was also spatially modulated (**Fig. 6**, third row). Full width at half minimum varied with saccade target location, $F(3, 240) = 8.40$, $p = 2.50 \times 10^{-5}$, and distractor location, $F(3, 240) = 7.60$, $p = 7.07 \times 10^{-5}$, with no interaction, $F(9, 240) < 1$. Bayesian model comparison provided strong evidence favoring the additive model, BF_{01} = 47.21. The target-location effect was limited: upward saccades exhibited a narrower inhibitory dip than rightward saccades, mean difference = 6.21 ms, adjusted $p = 2.64 \times 10^{-5}$.

By contrast, the distractor-location effect mirrored the inhibition-strength pattern. Upper-field distractors produced broader inhibition than lower-field distractors; all upper-versus-lower comparisons survived Holm adjustment, whereas left–right comparisons within the same vertical field did not.

Because directional-error saccades were excluded during preprocessing, we also tested whether this criterion could account for the spatial effects in the primary SI measures. Restoring otherwise eligible trials excluded solely because of saccade direction preserved the principal effects of saccade target and distractor location on inhibition strength, dip latency, and inhibition duration, see **Supplementary Analysis**.

JNeurosci Accepted Manuscript

Rebound Analysis

The rebound phase largely mirrored the inhibitory dip. Rebound peak amplitude varied with saccade target location, $F(3, 240) = 14.68$, $p = 8.24 \times 10^{-9}$, and distractor location, $F(3, 240) = 13.88$, $p = 2.23 \times 10^{-8}$. These factors did not interact, $F(9, 240) = 1.31$, $p = .232$, and Bayesian model comparison provided evidence favoring the additive model, $BF_{01} = 10.49$. Rebound peaks were smallest for upward saccades and largest for rightward saccades. Holm-adjusted comparisons showed that rightward saccades (0.416 ± 0.042) exhibited larger rebounds than upward (0.271 ± 0.029), downward (0.327 ± 0.027), and leftward (0.325 ± 0.034) saccades, and that leftward saccades exhibited larger rebounds than upward saccades. Distractor location again produced an upper-field pattern: rebound peaks were larger for upper-right (0.373 ± 0.032) and upper-left (0.396 ± 0.035) distractors than for lower-left (0.283 ± 0.025) and lower-right (0.287 ± 0.024) distractors. All upper-versus-lower distractor comparisons survived Holm adjustment. Thus, spatial conditions associated with stronger inhibition also showed larger post-inhibitory rebounds. Unlike rebound peak magnitude, rebound peak latency did not show reliable spatial modulation. It was not affected by saccade target location, $F(3, 240) < 1$, distractor location, $F(3, 240) = 2.11$, $p = .100$, or their interaction, $F(9, 240) = 1.04$, $p = .412$.

We next examined the rate of recovery from the inhibitory minimum to the rebound peak. Recovery slope varied with saccade target location, $F(3, 240) = 14.02$, $p = 1.89 \times 10^{-8}$, and distractor location, $F(3, 240) = 5.91$, $p = 6.58 \times 10^{-4}$, with no interaction, $F(9, 240) < 1$. Recovery was steeper for rightward (0.0223 ± 0.0028) than upward saccades (0.0136 ± 0.0013, $p = 1.50 \times 10^{-9}$), and downward (0.0172 ± 0.0016, $p = 1.16 \times 10^{-4}$) and leftward saccades (0.0170 ± 0.0018, $p = 7.42 \times 10^{-4}$) were intermediate. Upper-field distractors (upper-

JNeurosci Accepted Manuscript

548 right, 0.0188 ± 0.0018; upper-left, 0.0201 ± 0.0019) also produced steeper recovery than
549 lower-field distractors (lower-left, 0.0152 ± 0.0014; lower-right, 0.0159 ± 0.0015; all $p < .05$).

550

551 To determine whether the slope effect reflected a larger recovery trajectory or a shorter
552 recovery interval, we decomposed recovery into its vertical and temporal components. The
553 inhibitory-minimum-to-rebound-peak recovery amplitude varied with saccade target location,
554 $F(3, 240) = 23.58$, $p = 2.07 \times 10^{-13}$, and distractor location, $F(3, 240) = 19.39$, $p = 2.71 \times 10^{-11}$,
555 with no interaction, $F(9, 240) < 1$. Recovery excursions were largest for rightward saccades
556 and upper-field distractors. By contrast, the recovery interval was not modulated by saccade
557 target location, $F(3, 240) < 1$, distractor location, $F(3, 240) < 1$, or their interaction, $F(9, 240) <$
558 1. The spatial modulation of recovery slope was therefore driven primarily by the size of the
559 recovery excursion, rather than by a consistent change in the time required to reach the
560 rebound peak.

561

562 Rebound duration provided only weak evidence for spatial modulation. The duration of the
563 post-minimum above-baseline rebound was not reliably affected by saccade target location,
564 $F(3, 240) = 1.01$, $p = .391$, or by its interaction with distractor location, $F(9, 240) = 1.03$, $p =$
565 .419. Distractor location reached significance, $F(3, 240) = 3.64$, $p = .013$, but this effect was
566 supported by only one Holm-adjusted pairwise comparison, upper-left versus lower-right, $p =$
567 .027. We therefore did not use rebound duration as a central measure of the rebound profile.

568

569 **Target-distractor proximity**

570

571 Lastly, we tested whether the spatial pattern of SI could be explained by target–distractor
572 proximity. Because targets and distractors were presented at the same eccentricity, for each

JNeurosci Accepted Manuscript

saccade target two distractor locations were relatively near the target (45° angular separation) and two were relatively far (135° angular separation). We therefore recoded distractor conditions as near or far and analyzed the SI measures with saccade target location, proximity, and their interaction. There was no overall effect of proximity on inhibition strength, $F(1, 105) < 1$, $p = .688$, dip latency, $F(1, 105) = 1.38$, $p = .243$, or inhibition duration, $F(1, 105) = 1.47$, $p = .228$. Proximity nevertheless interacted with saccade target location for inhibition strength, $F(3, 105) = 5.59$, $p = .0013$, dip latency, $F(3, 105) = 8.07$, $p = 6.92 \times 10^{-5}$, and inhibition duration, $F(3, 105) = 3.52$, $p = .0176$. Critically, these interactions did not reflect a consistent advantage for near distractors. For inhibition strength, near distractors produced stronger inhibition for upward saccades, whereas the pattern reversed for downward saccades, with little near–far difference for leftward or rightward saccades. This reversal corresponds to the absolute upper–lower distractor-location asymmetry described above: for upward targets the near distractors were the two upper-field locations, whereas for downward targets those same upper-field locations constituted the far conditions. Thus, the spatial organization of SI in Experiment 1 could not be reduced to a general effect of target–distractor proximity.

Radial orientation bias

A stimulus-related factor to consider is the radial orientation bias, whereby peripheral orientation sensitivity depends on the relation between the stimulus orientation and the local radial axis, typically yielding greater sensitivity for radially than tangentially aligned stimuli (Westheimer, 2003). However, orientation in our protocol was task irrelevant: observers executed only the instructed saccade to the target and performed no perceptual judgment. Moreover, a radial orientation bias cannot account for the observed directional pattern; inhibition was stronger for rightward than leftward saccades but weaker for upward than downward saccades, despite matched radial–tangential alignment within each meridian. Radial alignment also fails to explain the distractor-location effects, because the vertically

JNeurosci Accepted Manuscript

oriented distractors at the four intercardinal locations shared equivalent oblique relations to the local radial axis.

Together, the results showed that saccadic inhibition was spatially anisotropic in both strength and temporal profile. The direction of the planned saccade modulated inhibition strength, whereas distractor location robustly shaped the strength, timing, and temporal width of the inhibitory response. The distractor-location effect was especially field-organized: upper-field distractors produced stronger, earlier, and broader inhibition than lower-field distractors. The rebound following inhibition corresponded to this pattern. Rebound amplitude and recovery slope were largest for rightward saccades and upper-field distractors, whereas rebound timing did not vary reliably across locations. Across the primary SI measures, interactions between saccade target location and distractor location were not reliable, and Bayesian model comparisons favored additive over interaction models, indicating that the contribution of each spatial factor was largely independent of the specific level of the other. This evidence was strongest for temporal width and rebound amplitude, and weaker for inhibition strength and dip latency. Thus, in Experiment 1, saccade target location and distractor location both influenced SI, but they did so largely independently rather than through specific target–distractor configurations.

Experiment 2: Intercardinal targets and cardinal distractors

Inhibition Analysis

Experiment 1 tested how saccadic inhibition depended on cardinal saccade targets and intercardinal distractors. Experiment 2 reversed this arrangement, placing saccade targets at

JNeurosci Accepted Manuscript

intercardinal locations and distractors along the cardinal axes. Distractor-present trials produced the same distractor-locked suppression and rebound relative to matched no-distractor baselines (Fig. 4B). We therefore focused on whether inhibition strength and timing were modulated by the planned saccade endpoint, the distractor location, or the spatial configuration of the target and distractor together.

Inhibition strength, indexed by the minimum of the SI profile, was spatially anisotropic (Fig. 7). It varied with saccade target location, $F(3, 240) = 7.37$, $p = 9.56 \times 10^{-5}$, and distractor location, $F(3, 240) = 17.67$, $p = 2.14 \times 10^{-10}$. Unlike Experiment 1, there was a reliable interaction between these factors, $F(9, 240) = 3.95$, $p = 8.67 \times 10^{-5}$.

To characterize this interaction, we tested the effect of distractor location separately for each saccade target location (Fig. 8A). Distractor location reliably modulated inhibition for upper-left targets, $F(3, 240) = 10.70$, $p = 3.77 \times 10^{-6}$, and upper-right targets, $F(3, 240) = 16.78$, $p = 2.52 \times 10^{-9}$, but not for lower-left or lower-right targets. Holm-adjusted pairwise comparisons showed that, for upper-right targets, the upper distractor produced stronger inhibition than the lower, left, and right distractors. For upper-left targets, the upper distractor also produced stronger inhibition than the lower distractor.

For the effect of saccade direction on each distractor location, inhibition was weaker for upper field saccade targets than lower targets for lower distractors, $F(3, 240) = 12.80$, $p = 3.49 \times 10^{-7}$, and right distractors, $F(3, 240) = 4.16$, $p = .0202$, all Holm-adjusted $p \leq 4.24 \times 10^{-4}$ (Fig. 8B).

JNeurosci Accepted Manuscript

The timing of maximal inhibition showed a more selective pattern (Fig. 7) Dip latency varied reliably with distractor location, $F(3, 240) = 7.74$, $p = 5.87 \times 10^{-5}$, but not with saccade target location, $F(3, 240) = 1.85$, $p = .139$, and the two factors did not interact, $F(9, 240) < 1$. Holm-adjusted comparisons showed that upper distractors (91.58 ± 1.35 ms) produced earlier inhibitory minima than lower (98.58 ± 1.92 ms) and left distractors (98.14 ± 1.57 ms), both $p \leq 6.77 \times 10^{-4}$. Inhibition strength depended jointly on target location and distractor location, but the timing of maximal inhibition was driven primarily by distractor location.

Dip onset showed a similar spatial pattern. Onset varied with distractor location, $F(3, 237.10) = 9.23$, $p = 8.43 \times 10^{-6}$, but not with saccade target location, $F(3, 237.18) = 2.12$, $p = .0983$, and these factors did not interact, $F(9, 237.10) = 1.57$, $p = .126$. Holm-adjusted comparisons showed earlier inhibition onset for upper distractors than for lower (mean difference = 11.27 ms, $p = 1.33 \times 10^{-5}$), left (9.72 ms, $p = 2.32 \times 10^{-4}$), and right distractors (6.30 ms, $p = .0297$). None of the remaining distractor-location comparisons was reliable after Holm correction (all adjusted $p \geq .102$). Thus, as in Experiment 1, dip onset was driven primarily by distractor location, with upper-field distractors producing the earliest inhibition.

The temporal width of inhibition did not show reliable asymmetries. Full width at half minimum was not affected by saccade target location, $F(3, 240) = 1.31$, $p = .273$, distractor location, $F(3, 240) < 1$, or their interaction, $F(9, 240) < 1$.

We conducted the same analysis of directional-error exclusions as in Experiment 1. Restoring otherwise eligible trials excluded solely because of saccade direction did not materially alter the principal SI results, including the reliable effects of saccade target and distractor location on inhibition strength and their interaction, see Supplementary analysis.

JNeurosci Accepted Manuscript

674

675 **Rebound Analysis**

676

677 The rebound phase largely mirrored the spatial structure of the inhibitory dip. Rebound peak
678 amplitude varied with saccade target location, $F(3, 240) = 4.29$, $p = .00571$, distractor location,
679 $F(3, 240) = 22.62$, $p = 6.21 \times 10^{-13}$, and their interaction, $F(9, 240) = 2.56$, $p = .00782$. Follow-
680 up analyses showed that distractor location modulated rebound amplitude for upper-right
681 targets, $F(3, 240) = 14.67$, Holm-adjusted $p = 3.35 \times 10^{-8}$, and upper-left targets, $F(3, 240) =$
682 9.54, Holm-adjusted $p = 1.70 \times 10^{-5}$, but not reliably for lower-field targets, Holm-adjusted $p >$
683 .05. Thus, as for inhibition strength, the rebound was most strongly shaped by distractor
684 location when saccades were planned to the upper visual field.

685

686 Rebound peak latency showed a selective distractor-location effect. It was not reliably affected
687 by saccade target location, $F(3, 240) = 2.06$, $p = .107$, and there was no reliable interaction,
688 $F(9, 240) = 1.45$, $p = .169$. However, rebound peak latency varied with distractor location, $F(3,$
689 $240) = 4.64$, $p = .00356$. Holm-adjusted comparisons showed that rebound peaks occurred
690 earlier for upper distractors (141.83 ± 3.32 ms) than for lower (152.89 ± 4.28 ms), left (149.98
691 ± 3.67 ms), and right distractors (150.88 ± 3.93 ms).

692

693 We next examined the rate of recovery from the inhibitory minimum to the rebound peak.
694 Recovery slope varied with saccade target location, $F(3, 240) = 3.17$, $p = .025$, and distractor
695 location, $F(3, 240) = 18.65$, $p = 6.57 \times 10^{-11}$, with no reliable interaction, $F(9, 240) < 1$. Holm-
696 adjusted comparisons showed steeper recovery for lower-right (0.0213 ± 0.0022) than upper-
697 left targets (0.0173 ± 0.0019), $p = .012$, and for upper distractors than lower, left, and right
698 distractors, all $p < .001$.

JNeurosci Accepted Manuscript

Then we asked whether the recovery-slope effect reflected a larger recovery excursion or a shorter recovery interval. Recovery amplitude, defined as the change from the inhibitory minimum to the rebound peak, varied with saccade target location, $F(3, 240) = 7.21$, $p = 1.19 \times 10^{-4}$, distractor location, $F(3, 240) = 26.51$, $p = 7.63 \times 10^{-15}$, and their interaction, $F(9, 240) = 4.17$, $p = 5.05 \times 10^{-5}$. Follow-up analyses showed that distractor location modulated recovery amplitude for upper-right targets, $F(3, 240) = 21.03$, Holm-adjusted $p = 1.58 \times 10^{-11}$, and upper-left targets, $F(3, 240) = 13.34$, Holm-adjusted $p = 1.32 \times 10^{-7}$, with upper distractors producing the largest recovery excursions. In contrast, the recovery interval showed no reliable main effect of saccade target location, $F(3, 240) = 1.02$, $p = .384$, or distractor location, $F(3, 240) = 1.68$, $p = .172$. Although the interaction was reliable, $F(9, 240) = 2.06$, $p = .034$, follow-up analyses did not reveal a consistent change in recovery timing. Thus, recovery-slope differences primarily reflected the size of the recovery excursion rather than the time needed to reach the rebound peak.

Target-distractor proximity

We also asked whether target-relative proximity could explain the target–distractor interaction in inhibition strength. For each saccade target, distractors separated by 45° were classified as near and those separated by 135° as far. There was an interaction between proximity and saccade target location, $F(3, 105) = 6.97$, $p = 2.54 \times 10^{-4}$. The near–far difference was pronounced for upper-field targets (upper-right: mean difference = 0.205 pp, $t(15) = 4.67$, Holm-adjusted $p = .0012$; upper-left: mean difference = 0.181 pp, $t(15) = 4.66$, Holm-adjusted $p = .00121$), but negligible for lower-field targets (lower-left: mean difference = −0.023 pp, $t(15) = -0.74$, Holm-adjusted $p = .942$; lower-right: mean difference = 0.012 pp, $t(15) = 0.41$, Holm-adjusted $p = .942$). Thus, proximity did not produce a consistent spatial pattern across

JNeurosci Accepted Manuscript

saccade targets and could not account for the target–distractor interaction observed in Experiment 2.

In Experiment 2, reversing the stimulus geometry altered the relation between orientation and location. The horizontally oriented targets appeared at intercardinal locations and were oblique to the local radial axis, whereas the vertically oriented distractors were radially aligned at the upper and lower locations but tangentially aligned at the left and right locations. Although a radial orientation bias (Westheimer, 2003) could have contributed to a general difference between vertical- and horizontal-meridian distractors, it cannot explain the stronger effects of the distractors at the upper than lower vertical meridian, nor can it account for the interaction between target and distractor locations.

The results in this experiment showed that reversing the target–distractor geometry changed the spatial organization of SI. Inhibition strength and rebound amplitude both depended on the pairing between saccade target and distractor locations, with the strongest upper-distractor effects emerging for upper-field targets. Dip latency was driven primarily by distractor location, whereas the temporal width of inhibition showed no reliable spatial modulation. Rebound recovery followed the same spatial pattern: recovery was steepest for lower-right targets and upper distractors, and this effect was driven mainly by larger recovery excursions rather than shorter recovery intervals.

Relation between SRT and SI across the visual field

To examine whether SI features were related to baseline SRT across visual-field locations, we matched, for each observer, the median no-distractor SRT at each target location with the

JNeurosci Accepted Manuscript

SI elicited by a distractor at the same location in the complementary experiment. SRT and SI measures were separately z-scored across the eight locations within each observer before computing correlations. Associations with baseline SRT were modest for inhibition magnitude, $r(126) = -.190$, $p = .032$, Holm-corrected $p = .091$; dip latency, $r(126) = .210$, $p = .018$, Holm-corrected $p = .070$; and dip onset, $r(125) = .192$, $p = .030$, Holm-corrected $p = .091$. Dip duration was not associated with baseline SRT, $r(126) = .001$, p and Holm-corrected $p = .994$ (Supplemental Fig. S3).

Together, the results in both experiments showed that SI remained spatially anisotropic when the target–distractor geometry was reversed, but its organization differed from that observed in Experiment 1. Unlike the additive spatial effects observed in Experiment 1, Experiment 2 revealed configuration-dependent interactions in inhibition strength and rebound amplitude, whereas the timing of SI was governed primarily by distractor location. Inhibition strength depended jointly on saccade target location and distractor location, with upper-field distractors producing particularly strong inhibition for upper-field saccade targets.

Discussion

Across two complementary spatial geometries, saccadic inhibition was not spatially uniform. Its strength, timing, and recovery depended on both the planned saccade endpoint and the interrupting visual transient's location. Thus, SI reflects a dynamic interaction between abrupt visual input and ongoing motor plans as a function of the location of the saccade target and the location of the distractor.

JNeurosci Accepted Manuscript

774 The two experiments revealed shared and geometry-dependent spatial structures. In
775 Experiment 1–cardinal saccade targets, intercardinal distractors–inhibition strength was
776 modulated additively by both the planned saccade direction and distractor location, such that
777 each location factor influenced inhibition without modifying the effect of the other. In
778 Experiment 2, reversing this spatial assignment–cardinal distractors and intercardinal targets–
779 yielded a reliable interaction between these factors. Thus, a distractor's interruptive effect
780 depended on both its location and the current saccade plan. Although very rare, directional
781 errors (0.66%) were more frequent on distractor-present (0.79%) than distractor-absent
782 (0.17%) trials and were preferentially directed toward the distractor (Supplementary Results),
783 consistent with interference affecting both saccade timing and selection. These findings
784 extend standard accounts of SI as a rapid sensory-driven interruption (Reingold & Stampe,
785 2002; Buonocore & McIntosh, 2008; McIntosh & Buonocore, 2014). They show that this
786 interruption is spatially structured and cannot be fully characterized by target-relative distractor
787 position alone; the absolute visual-field locations of both the planned endpoint and the
788 transient also matter.

789

790 The most consistent spatial effect was driven by distractor location: upper-field distractors
791 produced stronger inhibition and earlier inhibitory minima than lower-field distractors across
792 both experiments. This pattern diverges from classic fixation-based perceptual polar-angle
793 asymmetries—better performance along the horizontal than vertical meridian and along the
794 lower than upper vertical meridian at threshold and suprathreshold levels (Carrasco et al.,
795 2001; Talgar & Carrasco, 2002; Baldwin et al., 2012; Greenwood et al., 2017; Himmelberg et
796 al., 2020; Barbot et al., 2021; Hanning et al., 2022, 2024; Jigo et al., 2023). Instead, abrupt
797 upper-field transients exert a particularly strong influence on ongoing saccade preparation,
798 regardless of eye movement direction.

799

JNeurosci Accepted Manuscript

A potential neural substrate for this pattern is the superior colliculus (SC), a structure involved in visual processing, target selection, and saccade control. Nonhuman primate SC visual responses are sharper, stronger, and faster for upper-field stimuli, and peri-saccadic visual performance can also favor the upper visual field (Hafed & Chen, 2016; Fracasso et al., 2023; Hafed et al., 2023). Upper-field distractors may thus evoke stronger SC activity, producing earlier, more pronounced saccade preparation interruptions. The spatial-frequency content may also have contributed, because upper-field prefers higher spatial frequencies than lower-field SC (Hafed & Chen, 2016; Chen et al., 2018). By contrast, SC saccade-related motor burst is weaker for the upper-visual field (Hafed & Chen, 2016). Whether this asymmetry is related to the weaker inhibition of upward saccades remains unclear. These tentative interpretations based on the present behavioral data highlight the need to identify the neural source of this asymmetry in humans, especially given that asymmetries in the SC differ dramatically across species (for review, Hoy & Farrow, 2025). Moreover, it remains unknown whether neurophysiological data from nonhuman primates translate directly to humans. For instance, the vertical-meridian asymmetry in motion discrimination is opposite in human and nonhuman primates, likely due to their distinct ecological niches (Tuncok, Kiorpes & Carrasco, 2025).

The rapid timing of SI suggests that early visual transients reaching the oculomotor system may contribute to the inhibitory response (Bompas & Sumner, 2011; Bompas et al., 2020, 2025). Accordingly, dip onset is faster for stimuli with physical properties that decrease the latency of visually-driven spikes in the SC, such as higher luminance and low spatial frequency (Bompas, Sumner & Hedge, 2025). Although the physical properties of the distractors were identical across locations, the physiological responses they evoked are not necessarily uniform. Spatial differences in the strength or timing of these early visual responses could therefore contribute to the stronger and earlier inhibition elicited by upper-field distractors. However, Experiment 1, distractors at intercardinal locations should be perceived as having

JNeurosci Accepted Manuscript

827 the same strength and with similar timing. In Experiment 2, the strongest inhibition was caused
828 when the distractor was presented at the least salient and slowest location (review,
829 Himmelberg et al., 2023b).

830

831 The dissociation between inhibition strength and dip latency further suggests that distinct
832 spatial signals govern different SI components. Across both experiments, both dip latency and
833 dip onset were driven primarily by distractor location, reflecting sensory timing, whereas
834 inhibition strength depended on both the distractor location and saccade endpoint, reflecting
835 dynamic interaction of the sensory transient with the current motor plan. The cross-experiment
836 correlations lend further support to this interpretation. Locations associated with shorter
837 baseline SRTs showed stronger inhibition, earlier dip onset, and earlier inhibitory minima
838 (Supplemental Fig. S3), paralleling findings previously observed with contrast manipulations
839 (Bompas & Sumner, 2011). These results extend this relation from stimulus contrast to visual-
840 field location, aligning with spatial differences in the strength and timing of early visual signals
841 contributing to SI. Furthermore, the association with dip latency is also consistent with this
842 account, as the timing of maximal inhibition reflects both incoming visual input and its
843 subsequent interaction with ongoing saccade preparation. These timing measures capture
844 different stages of the inhibitory episode: dip onset marks its earliest measurable emergence,
845 whereas dip latency indicates the time of maximal inhibition, potentially reflecting subsequent
846 oculomotor dynamics.

847

848 Target-location effects point to the ongoing saccade plan's contribution. In Experiment 1,
849 upward saccades were least inhibited, and rightward saccades were most inhibited; in
850 Experiment 2, upper-field targets were again least inhibited, while lower-right targets reflected
851 stronger inhibition than either upper-left or upper-right targets. Thus, saccade plans vary in
852 vulnerability to interruption, a pattern distinct from canonical polar-angle asymmetries. These

JNeurosci Accepted Manuscript

853 effects cannot be explained simply by baseline timing differences; distractor timing was
854 calibrated per observer and target location, and SI profiles were computed relative to target-
855 location-matched no-distractor baselines. The weaker inhibition observed for upward
856 saccades aligns with reduced presaccadic attentional benefits before upward eye movements
857 (Hanning et al., 2022, 2024). Whether these effects arise from a shared mechanism remains
858 to be determined.

859

860 Comparing Experiments 1 and 2 indicates that SI depends on relative target–distractor
861 configuration, rather than isolated polar-angle locations. Saccade target and distractor location
862 effects were additive in Experiment 1 but interacted in Experiment 2, showing that neither
863 factor uniformly dominates SI; the same distractor location can have disparate consequences
864 depending on the planned saccade endpoint. Although target-relative geometry plays a role
865 (Buonocore & McIntosh, 2012), a simple proximity account based on near versus far target–
866 distractor separation cannot explain this interaction. Near–far differences were not consistent
867 across saccade target locations and were absent for lower-field targets in Experiment 2. This
868 pattern does not rule out competitive interactions within the SC. Rather, differences in the
869 strength of visual and saccade-related activity across locations could influence how distractor
870 signals interact with the ongoing saccade plan, potentially contributing to the different spatial
871 effects observed in the two experiments. Thus, target–distractor geometry operates against a
872 strong upper-field distractor bias; fully disentangling these factors will require orthogonally
873 manipulating polar angle and angular separation.

874

875 The complex target-distractor relation in Experiment 2 may partly reflect oblique saccades
876 engaging both horizontal and vertical saccade generation systems. Oblique saccades have
877 different properties (Becker & Jürgens, 1990; Nichols & Sparks 1996a,b) and are less frequent

JNeurosci Accepted Manuscript

than cardinal ones, reflecting allocentric environmental structure and oculomotor constraints (review, Reeves & Otero-Millan, 2026).

Post-inhibitory rebound largely mirrored the dip's spatial structure. Conditions with stronger inhibition tended to produce larger rebound peaks and steeper recovery slopes, particularly for upper-field distractors. The slope decomposition further clarified this pattern: steeper recovery was driven primarily by a larger excursion from the inhibitory minimum to the rebound peak, rather than by consistently shortened recovery intervals. This finding supports interpreting post-inhibitory rebound as recovery from strong inhibition, rather than as an independent facilitation mechanism (Dombrowe, 2018; Buonocore & Hafed, 2023).

The dissociation between SI and fixation-based perceptual visual field asymmetries is consistent with a growing body of work showing that active-vision phenomena depend strongly on task demands and behavioral state. For instance, presaccadic attention (Hanning et al., 2022, 2024; Kwak et al., 2024) and transsaccadic preview benefits (Liu et al., 2024) vary with saccade direction and visual-field location in ways that depend on the specific task and performance measures employed. The present results extend this logic to transient-driven oculomotor interruption, demonstrating that even low-level, reflex-like inhibitory mechanisms are shaped by the spatial context of the motor plan.

Because our task required no perceptual judgment about the distractor, the observed anisotropies characterize the rapid sensorimotor consequences of an abrupt transient rather than reflecting perceptual sensitivity. As perceptual strength need not predict sensorimotor impact (Budnik et al., 2013), spatial asymmetries in active vision may depend on the type and timing of visual information involved, as well as the behavioral state and the neural circuit being probed: perception, attention, saccade preparation, and transient-driven inhibition need

JNeurosci Accepted Manuscript

not share a common field map. This distinction is critical because it positions SI as a complementary assay of visual-field organization, one that probes how abrupt sensory events regulate ongoing action rather than how visual stimuli are perceived during fixation.

The current findings suggest several possible future directions. First, our experiments used task-irrelevant Gabor distractors in a speeded saccade task, allowing us to isolate visually driven interruption of saccade preparation. Future work should investigate whether the same spatial organization persists when the target or distractors are behaviorally relevant or embedded in a perceptual decision. Second, our protocol tested a single eccentricity, and the distractor was larger and lower in spatial frequency than the saccade target to elicit robust SI; future work should determine whether the same spatial pattern holds across manipulations of eccentricity, stimulus size, and spatial frequency. Third, although rightward saccades showed particularly strong inhibition in Experiment 1, additional work is needed to determine whether such effects reflect stable lateral differences in oculomotor preparation, hemispheric organization, reading direction, or individual experience. Finally, our behavioral results cannot identify the neural source of the observed asymmetries. The superior colliculus provides a plausible substrate, but neural measurements or targeted perturbations are needed to test this hypothesis directly.

To conclude, the present study shows that saccadic inhibition is spatially structured. Inhibition strength depends on both the planned saccade endpoint and the location of the interrupting distractor. By contrast, the timing of maximal inhibition is uniquely sensitive to distractor location, while the subsequent rebound primarily reflects recovery from the preceding inhibitory episode. By testing two complementary target–distractor geometries, we show that these spatial effects can be additive in one geometry and configuration-dependent in another.

JNeurosci Accepted Manuscript

Consequently, SI provides a powerful behavioral assay of how spatially anisotropic visual and oculomotor signals interact dynamically to regulate saccade generation during active vision.

Data Availability.

Raw eye-tracking and behavioral data supporting the findings of this study are available at https://github.com/CarrascoLab/SaccadicInhibPF.

Author contributions.

J.H., D.M., and M.C. designed research; J.H. performed research and analyzed the data; J.H., D.M., and M.C. interpreted the data; J.H. wrote the first draft of the paper; M.C. substantially edited the manuscript; D.M. provided feedback; J.H., D.M., and M.C. approved the final version of the paper.

Acknowledgments.

This research is funded by NIH R01-EY027401 to M.C. and Tamkeen under NYU Abu Dhabi Research Institute grant CG012 to DM. We thank Marc Himmelberg, Hsing-Hao Lee, and other members of the Carrasco Lab for their helpful comments.

JNeurosci Accepted Manuscript

References

Baldwin AS, Meese TS, Baker DH (2012) The attenuation surface for contrast sensitivity has the form of a witch's hat within the central visual field. J Vis 12:23.

Barbot A, Xue S, Carrasco M (2021) Asymmetries in visual acuity around the visual field. J Vis 21:2.

Basso MA, May PJ (2017) Circuits for action and cognition: a view from the superior colliculus. Annu Rev Vis Sci 3:197–226.

Becker W, Jürgens R (1990) Human oblique saccades: quantitative analysis of the relation between horizontal and vertical components. Vision Res 30:893–920.

Benson NC, Kupers ER, Barbot A, Carrasco M, Winawer J (2021) Cortical magnification in human visual cortex parallels task performance around the visual field. Elife 10.

Bompas A, Sumner P (2008) Sensory sluggishness dissociates saccadic, manual, and perceptual responses: an S-cone study. J Vis 8:10.

Bompas A, Sumner P (2011) Saccadic inhibition reveals the timing of automatic and voluntary signals in the human brain. J Neurosci 31:12501–12512.

Bompas A, Campbell AE, Sumner P (2020) Cognitive control and automatic interference in mind and brain: a unified model of saccadic inhibition and countermanding. Psychol Rev 127:524–561.

Bompas A, Sumner P, Hedge C (2025) Non-decision time: the Higgs Boson of decision. Psychol Rev 132:330–363.

Brainard DH (1997) The Psychophysics Toolbox. Spatial Vis 10:433–436.

Budnik U, Bompas A, Sumner P (2013) Perceptual strength is different from sensorimotor strength: evidence from the centre–periphery asymmetry in masked priming. Q J Exp Psychol (Hove) 66:15–22.

JNeurosci Accepted Manuscript

973 Buonocore A, McIntosh RD (2008) Saccadic inhibition underlies the remote distractor effect.
974 Exp Brain Res 191:117–122.

975 Buonocore A, McIntosh RD (2012) Modulation of saccadic inhibition by distractor size and
976 location. Vision Res 69:32–41.

977 Buonocore A, McIntosh RD (2013) Attention modulates saccadic inhibition magnitude. Q J
978 Exp Psychol (Hove) 66:1051–1059.

979 Buonocore A, Tian X, Khademi F, Hafed ZM (2021) Instantaneous movement-unrelated
980 midbrain activity modifies ongoing eye movements. Elife 10.

981 Buonocore A, Hafed ZM (2023) The inevitability of visual interruption. J Neurophysiol
982 130:225–237.

983 Carrasco M, Talgar CP, Cameron EL (2001) Characterizing visual performance fields: effects
984 of transient covert attention, spatial frequency, eccentricity, task and set size. Spatial Vis
985 15:61–75.

986 Carrasco M, Giordano AM, McElree B (2004) Temporal performance fields: visual and
987 attentional factors. Vision Res 44:1351–1365.

988 Chen C-Y, Sonnenberg L, Weller S, Witschel T, Hafed ZM (2018) Spatial frequency sensitivity
989 in macaque midbrain. Nat Commun 9:2852.

990 Cornelissen FW, Peters EM, Palmer J (2002) The EyeLink Toolbox: eye tracking with
991 MATLAB and the Psychophysics Toolbox. Behav Res Methods Instrum Comput 34:613–
992 617.

993 Curcio CA, Allen KA (1990) Topography of ganglion cells in human retina. J Comp Neurol
994 300:5–25.

995 Curcio CA, Sloan KR, Kalina RE, Hendrickson AE (1990) Human photoreceptor topography.
996 J Comp Neurol 292:497–523.

JNeurosci Accepted Manuscript

997 Dombrowe I (2018) Saccadic inhibition in a guided saccade task. PeerJ 6.

998 Edelman JA, Xu KZ (2009) Inhibition of voluntary saccadic eye movement commands by
999 abrupt visual onsets. J Neurophysiol 101:1222–1234.

1000 Fracasso A, Buonocore A, Hafed ZM (2023) Peri-saccadic orientation identification
1001 performance and visual neural sensitivity are higher in the upper visual field. J Neurosci
1002 43:6884–6897.

1003 Greenwood JA, Szinte M, Sayim B, Cavanagh P (2017) Variations in crowding, saccadic
1004 precision, and spatial localization reveal the shared topology of spatial vision. Proc Natl
1005 Acad Sci U S A 114–E3582.

1006 Hafed ZM, Chen C-Y (2016) Sharper, stronger, faster upper visual field representation in
1007 primate superior colliculus. Curr Biol 26:1647–1658.

1008 Hafed ZM, Hoffmann K-P, Chen C-Y, Bogadhi AR (2023) Visual functions of the primate
1009 superior colliculus. Annu Rev Vis Sci 9:361–383.

1010 Hanning NM, Himmelberg MM, Carrasco M (2022) Presaccadic attention enhances contrast
1011 sensitivity, but not at the upper vertical meridian. iScience 25:103851.

1012 Hanning NM, Himmelberg MM, Carrasco M (2024) Presaccadic attention depends on eye
1013 movement direction and is related to V1 cortical magnification. J Neurosci 44.

1014 Himmelberg MM, Winawer J, Carrasco M (2020) Stimulus-dependent contrast sensitivity
1015 asymmetries around the visual field. J Vis 20:18.

1016 Himmelberg MM, Kurzawski JW, Benson NC, Pelli DG, Carrasco M, Winawer J (2021) Cross-
1017 dataset reproducibility of human retinotopic maps. Neuroimage 244:118609.

1018 Himmelberg MM, Winawer J, Carrasco M (2022) Linking individual differences in human
1019 primary visual cortex to contrast sensitivity around the visual field. Nat Commun 13:3309.

JNeurosci Accepted Manuscript

Himmelberg MM, Tünçok E, Gomez J, Grill-Spector K, Carrasco M, Winawer J (2023a) Comparing retinotopic maps of children and adults reveals a late-stage change in how V1 samples the visual field. Nat Commun 14:1561.

Himmelberg MM, Winawer J, Carrasco M (2023b) Polar angle asymmetries in visual perception and neural architecture. Trends Neurosci 46:445–458.

Himmelberg MM, Kwak Y, Carrasco M, Winawer J (2025) Unpacking the V1 map: differential covariation of preferred spatial frequency and cortical magnification across spatial dimensions. PLoS Comput Biol 21.

Hoy JL, Farrow K (2025) The superior colliculus. Curr Biol 35:R164–R168.

Isa T, Hall WC (2009) Exploring the superior colliculus in vitro. J Neurophysiol 102:2581–2593.

Jantz JJ, Watanabe M, Everling S, Munoz DP (2013) Threshold mechanism for saccade initiation in frontal eye field and superior colliculus. J Neurophysiol 109:2767–2780.

Jigo M, Tavdy D, Himmelberg MM, Carrasco M (2023) Cortical magnification eliminates differences in contrast sensitivity across but not around the visual field. Elife 12:e84205.

Khademi F, Zhang T, Baumann MP, Buonocore A, Malevich T, Yu Y, Hafed ZM (2023) Visual feature tuning properties of stimulus-driven saccadic inhibition in macaque monkeys. J Neurophysiol 130:1282–1302.

Kupers ER, Carrasco M, Winawer J (2019) Modeling visual performance differences “around” the visual field: a computational observer approach. PLoS Comput Biol 15.

Kupers ER, Benson NC, Carrasco M, Winawer J (2022) Asymmetries around the visual field: from retina to cortex to behavior. PLoS Comput Biol 18.

Kwak Y, Zhao Y, Lu Z-L, Hanning NM, Carrasco M (2024) Presaccadic attention enhances and reshapes the contrast sensitivity function differentially around the visual field. eNeuro 11.0243-24.2024.

JNeurosci Accepted Manuscript

1044 Kwak Y, Hanning NM, Carrasco M (2025) Saccade direction modulates the temporal dynamics
1045 of presaccadic attention. J Vis 25:2.

1046 Liu X, Melcher D, Carrasco M, Hanning NM (2024) Presaccadic preview shapes postsaccadic
1047 processing more where perception is poor. Proc Natl Acad Sci U S A 121.

1048 McIntosh RD, Buonocore A (2014) Saccadic inhibition can cause the remote distractor effect,
1049 but the remote distractor effect may not be a useful concept. J Vis 14:15.

1050 Nichols MJ, Sparks DL (1996a) Component stretching during oblique stimulation-evoked
1051 saccades: the role of the superior colliculus. J Neurophysiol 76:582–600.

1052 Nichols MJ, Sparks DL (1996b) Independent feedback control of horizontal and vertical
1053 amplitude during oblique saccades evoked by electrical stimulation of the superior
1054 colliculus. J Neurophysiol 76:4080–4093.

1055 Pelli DG (1997) The VideoToolbox software for visual psychophysics: transforming numbers
1056 into movies. Spatial Vis 10:437–442.

1057 Reeves SM, Otero-Millan J (2026) Horizontal saccade bias results from combination of
1058 saliency anisotropies and egocentric biases. Sci Rep 16:6027.

1059 Reingold EM, Stampe DM (1999) Saccadic inhibition in complex visual tasks. In: Current
1060 oculomotor research: physiological and psychological aspects (Becker W, Deubel H,
1061 Mergner T, eds), pp 249–255. New York: Plenum.

1062 Reingold EM, Stampe DM (2002) Saccadic inhibition in voluntary and reflexive saccades. J
1063 Cogn Neurosci 14:371–388.

1064 Reingold EM, Stampe DM (2004) Saccadic inhibition in reading. J Exp Psychol Hum Percept
1065 Perform 30:194–211.

1066 Salinas E, Stanford TR (2018) Saccadic inhibition interrupts ongoing oculomotor activity to
1067 enable rapid reprogramming of movement plans. Sci Rep 8:14163.

JNeurosci Accepted Manuscript

1068 Silva MF, Brascamp JW, Ferreira S, Castelo-Branco M, Dumoulin SO, Harvey BM (2018)
1069 Radial asymmetries in population receptive field size and cortical magnification factor in
1070 early visual cortex. Neuroimage 167:41–52.

1071 Stampe DM, Reingold EM (2002) Influence of stimulus characteristics on the latency of
1072 saccadic inhibition. Prog Brain Res 140:73–87.

1073 Talgar CP, Carrasco M (2002) Vertical meridian asymmetry in spatial resolution: visual and
1074 attentional factors. Psychon Bull Rev 9:714–722.

1075 Tünçok E, Kiorpes L, Carrasco M (2025) Opposite asymmetry in visual perception of humans
1076 and macaques. Curr Biol 35:681–687.e4.

1077 Wagenmakers E-J, Marsman M, Jamil T, Ly A, Verhagen J, Love J, Selker R, Gronau QF,
1078 Šmíra M, Epskamp S, Matzke D, Rouder JN, Morey RD (2018) Bayesian inference for
1079 psychology. Part I: theoretical advantages and practical ramifications. Psychon Bull Rev
1080 25:35–57.

1081 Walker R, Benson V (2013) Remote distractor effect and saccadic inhibition: spatial and
1082 temporal modulation. J Vis 13:9.

1083 Walker R, Benson V (2015) Saccadic distractor effects: the remote distractor effect (RDE) and
1084 saccadic inhibition (SI): a response to McIntosh and Buonocore (2014). J Vis 15:6.

1085 Westheimer G (2003) The distribution of preferred orientations in the peripheral visual field.
1086 Vision Res 43:53–57.

1087

1088 **Figure Legends**

1089 **Figure 1. Characteristic saccadic inhibition (SI) time course**. Normalized saccade
1090 frequency is plotted as a function of time from transient (distractor) onset. A brief visual
1091 transient evokes a rapid, time-locked suppression of saccade probability, followed by a

JNeurosci Accepted Manuscript

rebound toward baseline. The vertical solid line marks distractor onset. The minimum denotes the point of maximal inhibition. *Strength* is defined as the depth of the minimum relative to baseline, *latency* as the interval from distractor onset to the minimum, and *duration* as the full width of the inhibitory dip at half minimum. Exact computational procedures are described in the Methods.

Figure 2. Task procedure and spatial configurations. **(A)** Trial sequence used in both experiments. Each trial began with central fixation for a jittered interval of 900-1500 ms, followed by the onset of a peripheral saccade target. The target remained visible for 400 ms. On distractor-present trials, a distractor appeared after target onset, with the target–distractor stimulus onset asynchrony (SOA) set to the observer and target location specific median calibration SRT minus 90 ms. The distractor remained visible for 250 ms. Observers made a speeded saccade to the target; the dashed red circle in the schematic indicates gaze position after the saccade. No-distractor trials followed the same sequence except that the distractor was omitted. Stimulus size, contrast, and the timeline are for illustration purposes and are not drawn to scale. **(B)** Spatial configuration in Experiment 1: saccade targets appeared at cardinal locations and distractors appeared at intercardinal locations. **(C)** Spatial configuration in Experiment 2: saccade targets appeared at intercardinal locations and distractors appeared at cardinal locations. Target and distractor locations were presented at 8.5° eccentricity.

Figure 3. Baseline saccade timing and endpoint distributions. **(A)** Observer-averaged median saccadic reaction times (SRTs) as a function of target location for Experiment 1 (cardinal targets; left) and Experiment 2 (intercardinal targets; right). Radial distance indicates median SRT in milliseconds. Solid and dashed traces show median SRTs from the main-session no-distractor trials and calibration trials, respectively. Error bars indicate ±1 SEM. **(B)** Normalized saccade endpoint frequency maps averaged across observers for Experiment 1 (left) and

JNeurosci Accepted Manuscript

Experiment 2 (right). Color indicates normalized endpoint frequency, with darker values corresponding to higher endpoint density.

Figure 4. Group-average saccade-rate and saccadic-inhibition profiles in Experiments 1 and 2. **(A)** Experiment 1. Top, saccade probability as a function of latency from distractor onset for distractor-present trials and matched no-distractor baseline trials. Bottom, overall SI profile computed as the difference between distractor-present and no-distractor saccade-probability distributions. **(B)** Experiment 2, plotted in the same format. Dashed gray lines show no-distractor baselines aligned to the corresponding pseudo-distractor onset; solid red lines show distractor-present trials; blue lines show the resulting SI profiles. All curves represent group means across the same 16 observers. Negative SI values indicate reduced saccade probability relative to baseline, and positive values indicate rebound above baseline.

Figure 5. Saccadic-inhibition profiles by saccade target location and distractor location in Experiment 1. **(A)** Saccadic-inhibition profiles plotted as a function of latency from distractor onset, separately for each saccade target location. Traces are collapsed across distractor locations. Negative values indicate reduced saccade probability relative to the matched no-distractor baseline, and positive values indicate rebound above baseline. **(B)** Saccadic-inhibition profiles plotted separately for each distractor location, collapsed across saccade target locations. All profiles were computed as the difference between distractor-present and target-location-matched no-distractor saccade-frequency distributions.

Figure 6. Inhibition strength, dip latency, inhibition duration, and dip onset by saccade target location and distractor location in Experiment 1. **(A)** SI measures plotted as a function of saccade target location, collapsed across distractor locations. **(B)** SI measures plotted as a function of distractor location, collapsed across saccade target locations. The four rows show

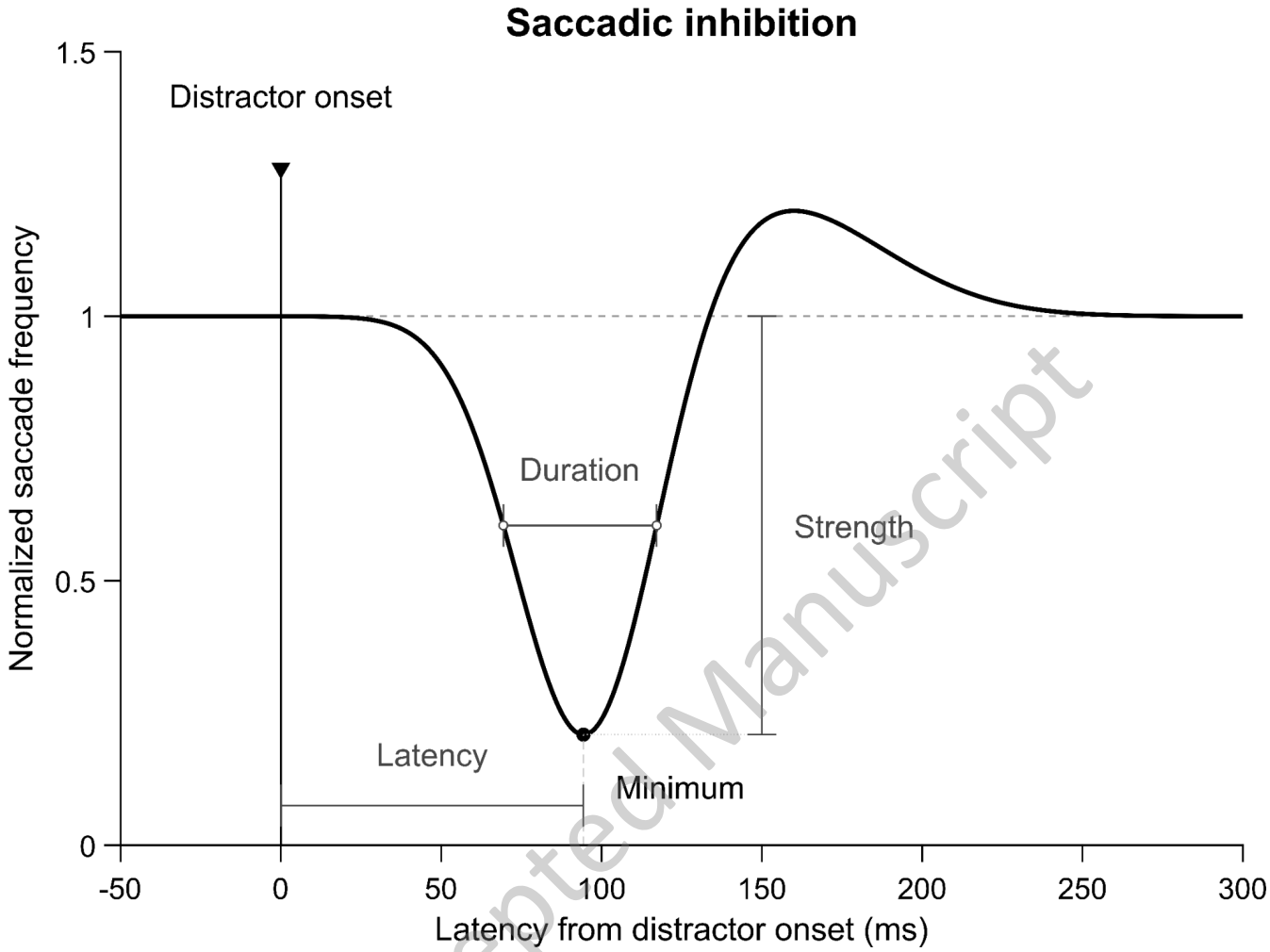
JNeurosci Accepted Manuscript

inhibition strength, defined as the minimum of the SI profile; dip latency, defined as the time of maximal inhibition relative to distractor onset; and inhibition duration, defined as the full width at half minimum; and dip onset, estimated using the 2% distraction-ratio criterion (see Methods). Gray points indicate individual-observer values, colored points indicate group means, and error bars indicate ±1 SEM. Brackets indicate Holm-corrected pairwise comparisons. Error bars centered on the comparison line segments indicate ±1 SEM of the difference between conditions. Significant pairwise comparisons were based on Holm-corrected LMM post hoc tests. ***$p < 0.001$; **$p < 0.01$; *$p < 0.05$.

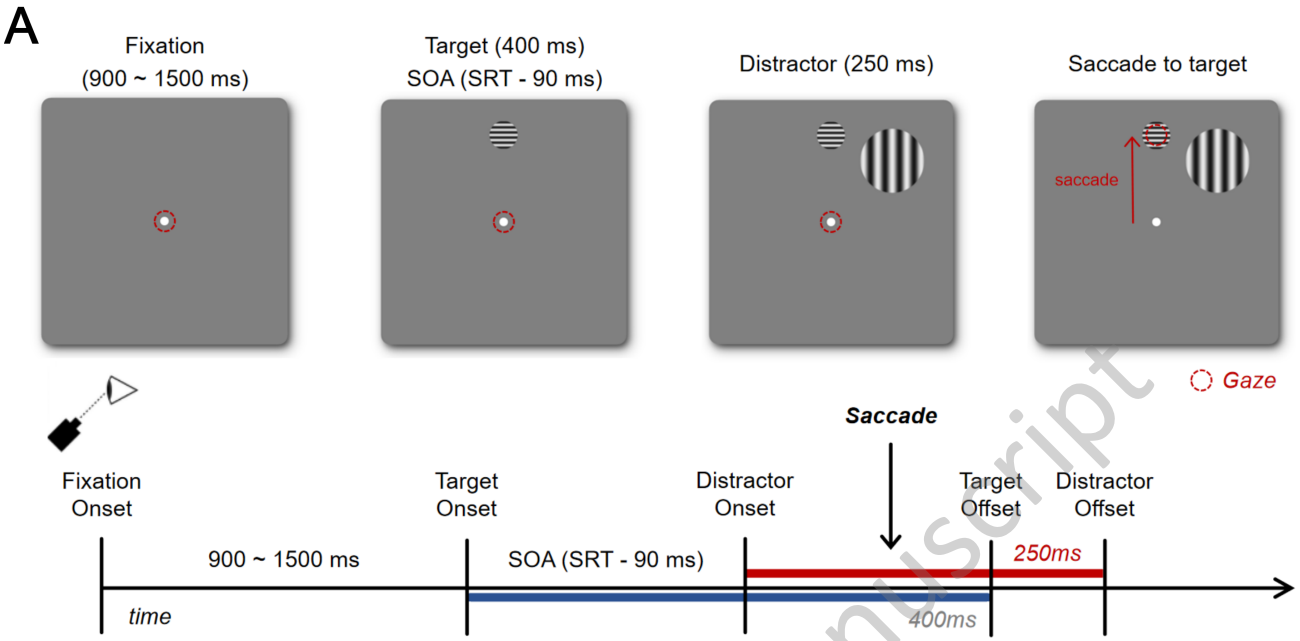
Figure 7. Saccadic-inhibition profiles by saccade target location and distractor location in Experiment 2. **(A)** SI profiles plotted separately by saccade target location and collapsed across distractor locations. **(B)** SI profiles plotted separately by distractor location and collapsed across saccade target locations. All profiles show the change in saccade probability relative to the matched no-distractor baseline as a function of latency from distractor onset.

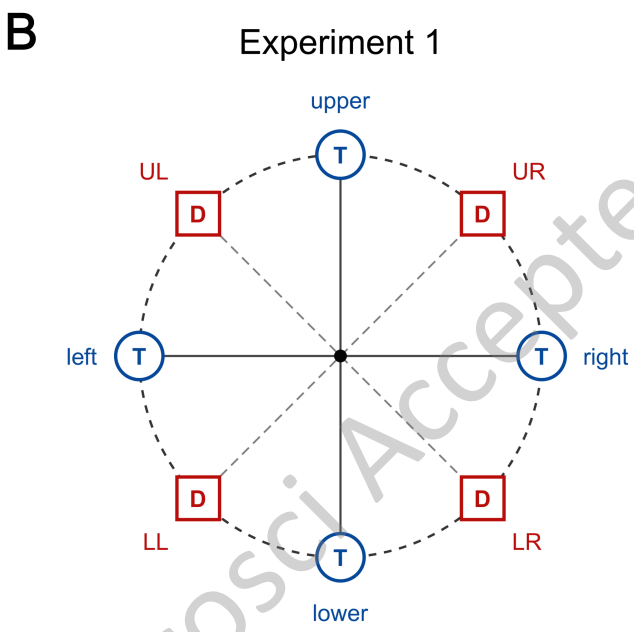
Figure 8. Conditional SI profiles across the target–distractor geometry in Experiment 2. **(A)** SI profiles plotted separately for each saccade target location, with traces corresponding to the four distractor locations. **(B)** SI profiles plotted separately for each distractor location, with traces corresponding to the four saccade target locations. These panels visualize the interaction between saccade target location and distractor location by showing how the distractor-location effect varied across planned saccade endpoints. Negative values indicate reduced saccade probability relative to the matched no-distractor baseline; positive values indicate rebound above baseline.

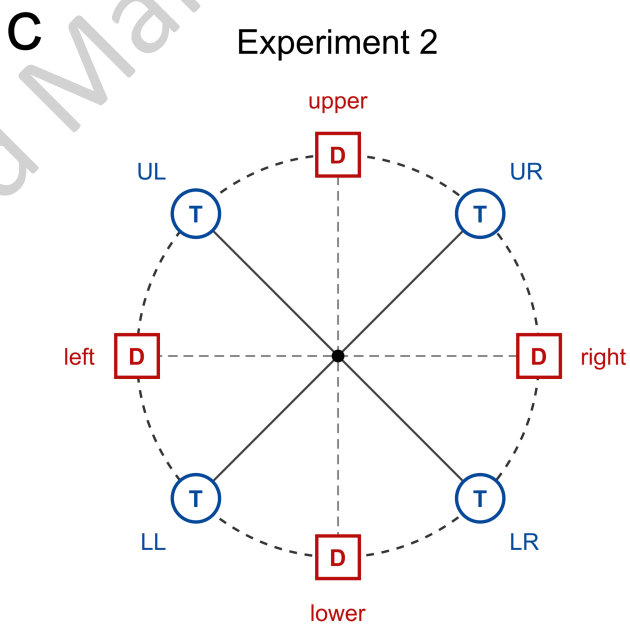
JNeurosci Accepted Manuscript



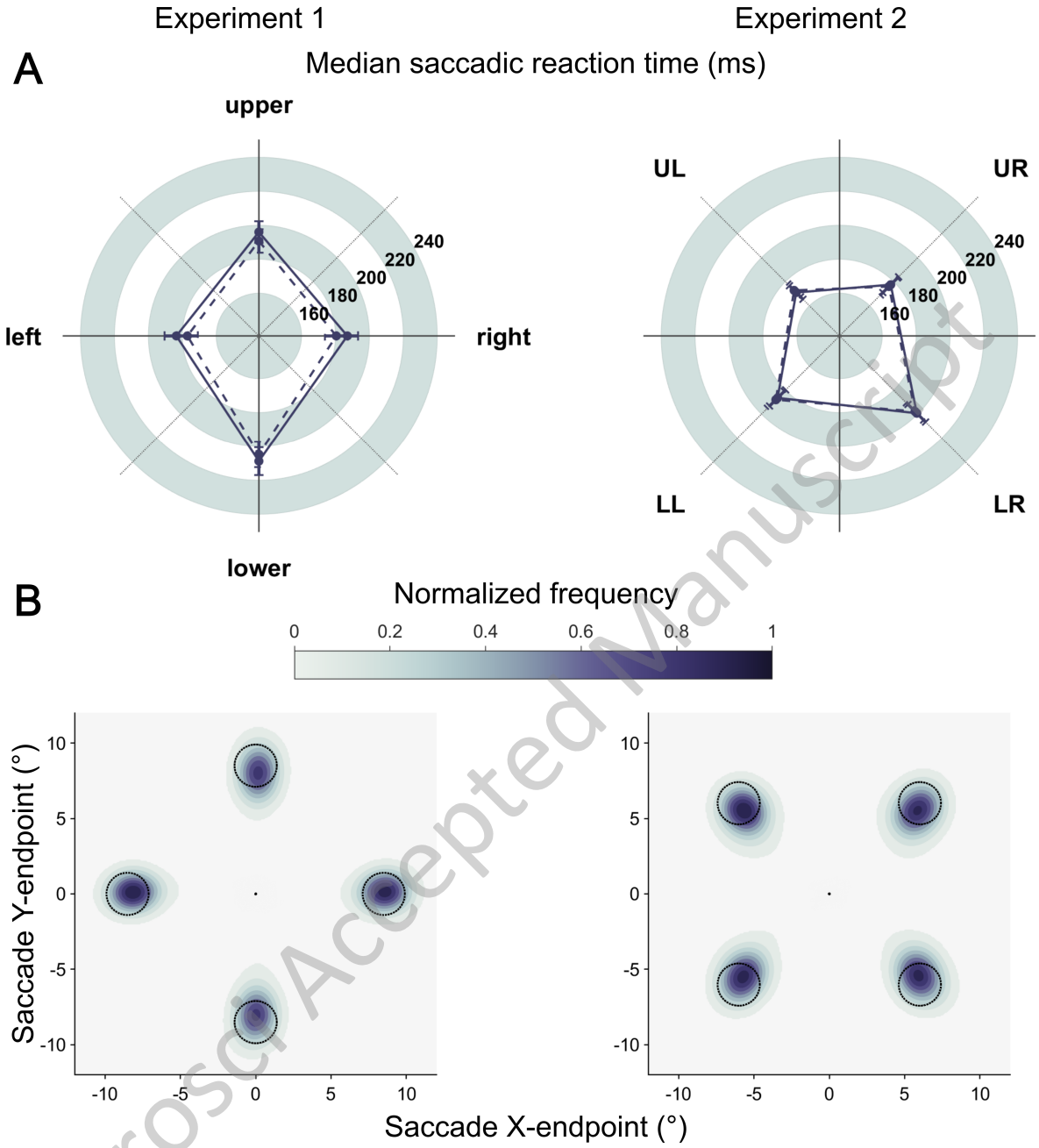
JNeurosci Accepted Manuscript



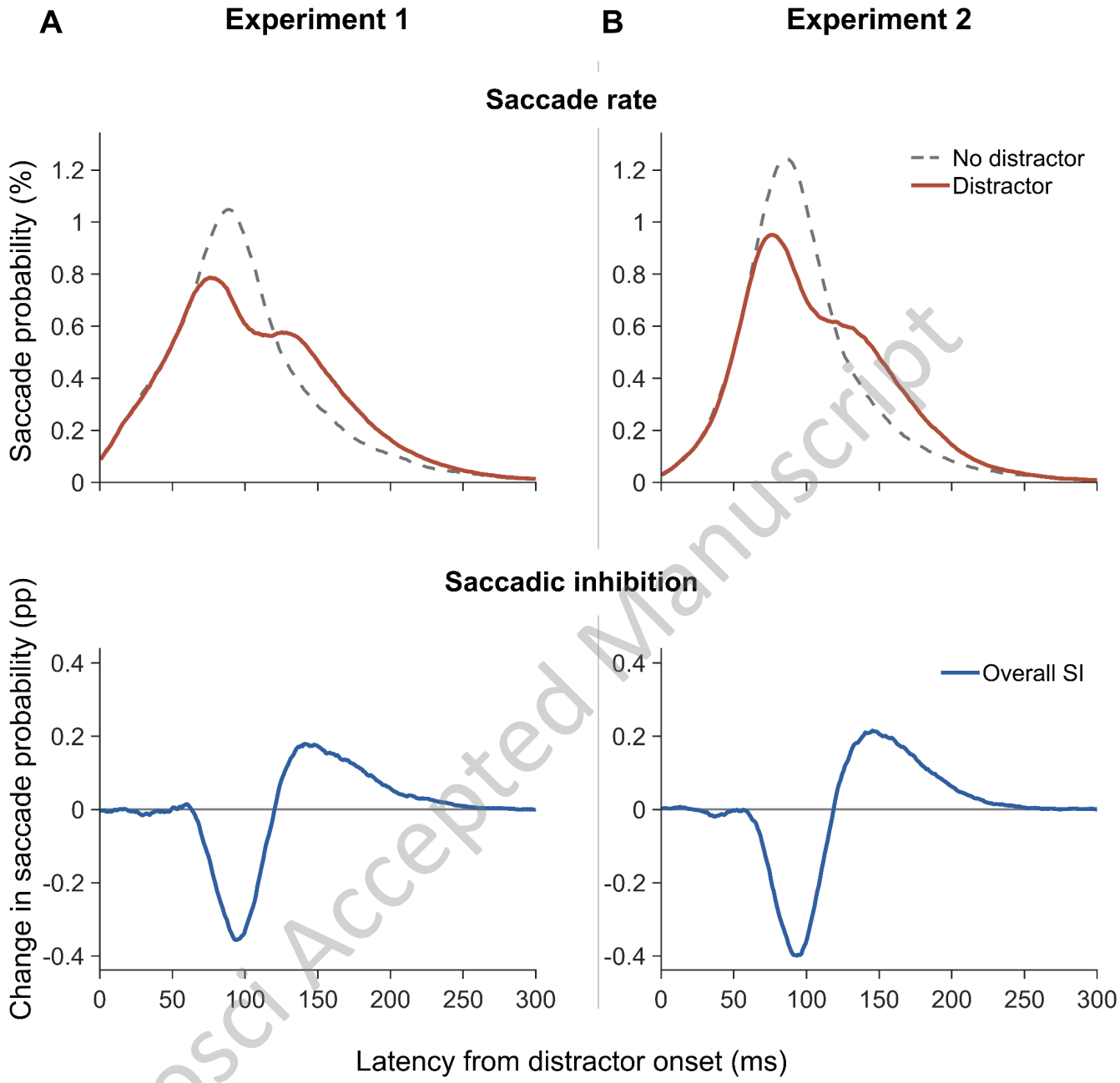




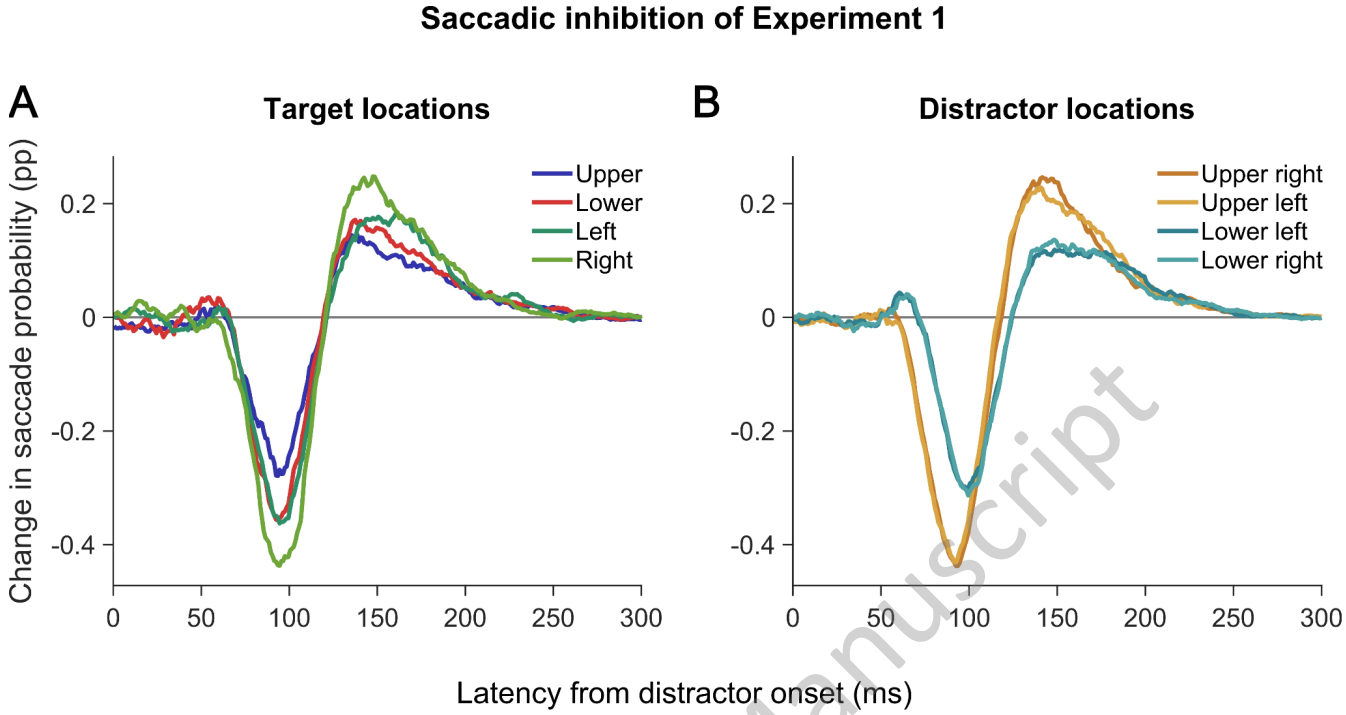
JNeurosci Accepted Manuscript



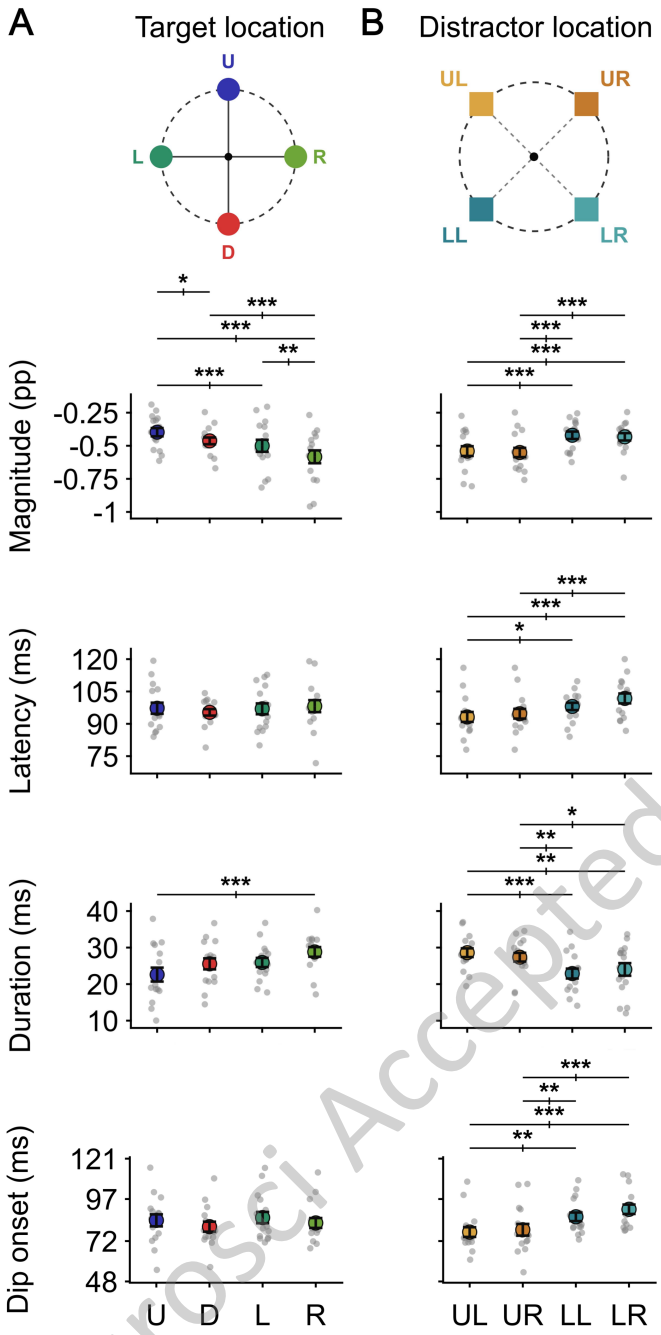
JNeurosci Accepted Manuscript



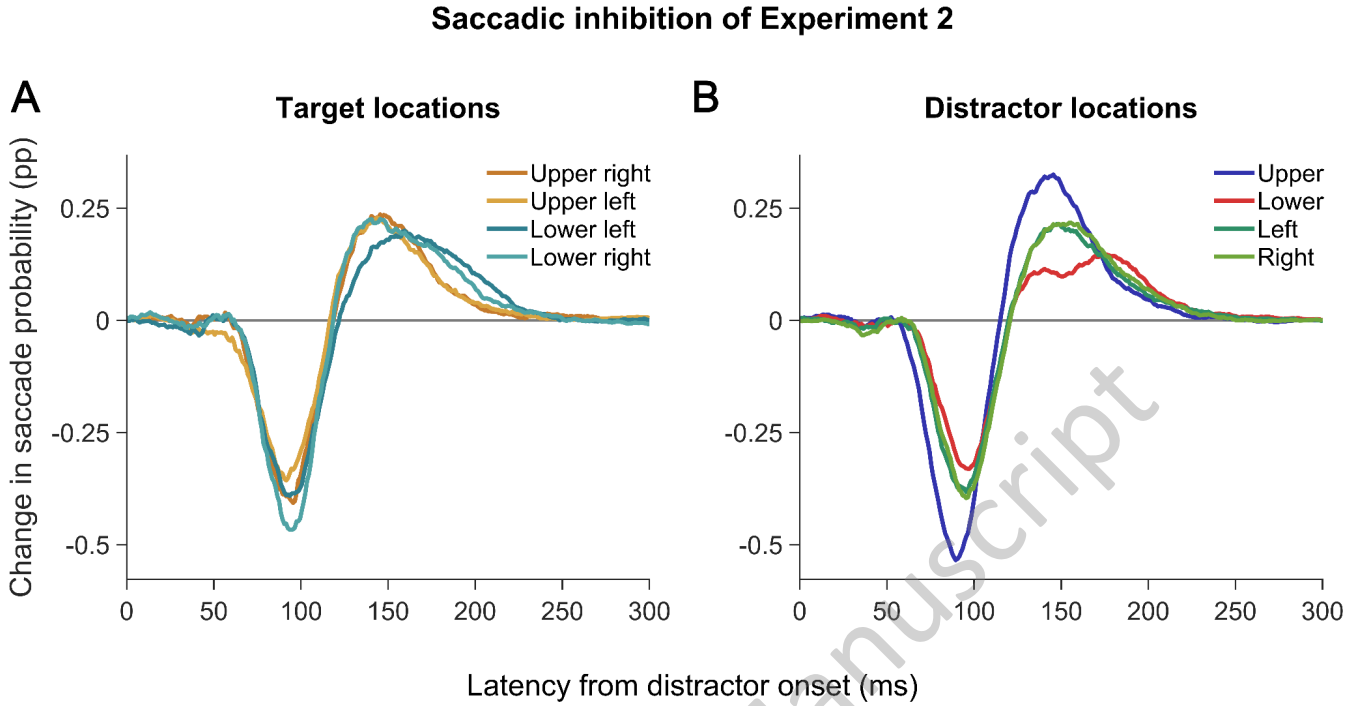
JNeurosci Accepted Manuscript



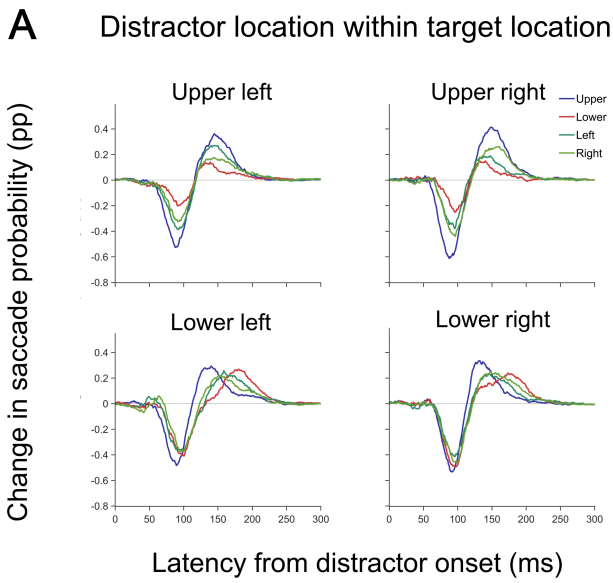
JNeurosci Accepted Manuscript

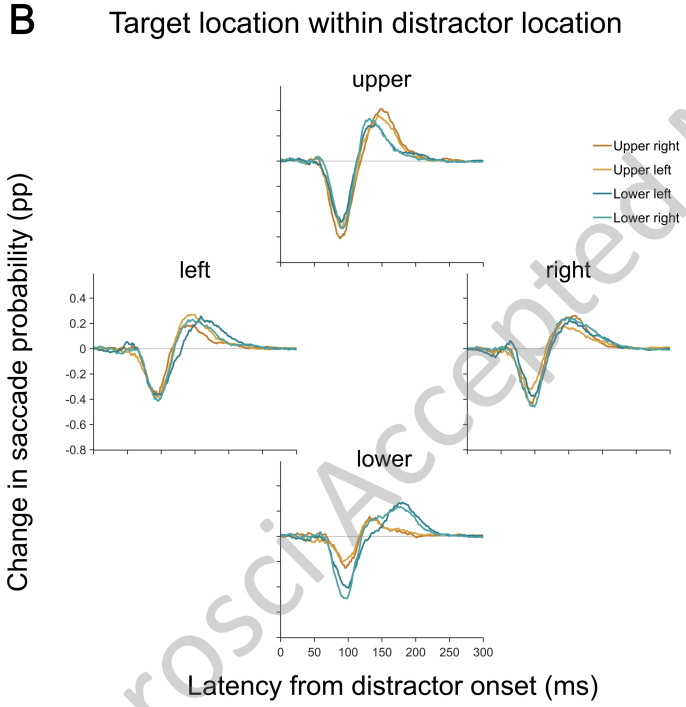


JNeurosci Accepted Manuscript



JNeurosci Accepted Manuscript





JNeurosci Accepted Manuscript